Insights from the Physicochemical and Electrochemical Screening of the Potentiality of the Chemically Synthesized Polyaniline

Razik Djara, Yaovi Holade, Abdelhafid Merzouki, Nathalie Masquelez, Didier Cot, Bertrand Rebière, Eddy Petit, Patrice Huguet, Christine Canaff, Sophie Morisset, et al.

Insights from the Physicochemical and Electrochemical Screening of the Potentiality of the Chemically Synthesized Polyaniline

Razik Djara,[a,b] Yaovi Holade,[b,z,*] Abdelhafid Merzouki,[a] Nathalie Masquelez,[b] Didier Cot,[b] Bertrand Rebiere,[c] Eddy Petit,[b] Patrice Huguet,[b] Christine Canaff,[d] Sophie Morisset,[d] Teko W. Napporn,[d,*] David Cornu,[b] and Sophie Tingry[b,z]

[a]*Laboratoire de Physico-Chimie des Hauts Polymères (LPCHP), Université Ferhat Abbas, Sétif 1, Algeria*

[b]*Institut Européen des Membranes, IEM – UMR 5635, ENSCM, CNRS, Univ Montpellier, Montpellier, France*

[c]*Institut Charles Gerhardt, UMR-5253, CNRS, ENSCM, Univ Montpellier, Montpellier, France*

[d] *Université de Poitiers, IC2MP UMR-CNRS 7285, 4 rue Michel Brunet, B27 – TSA 51106, 86073 Poitiers Cedex 9, France*

[z]Corresponding Author:yaovi.holade@enscm.fr(Y.H.), sophie.tingry@umontpellier.fr(S.T.)

*Electrochemical Society Member

Abstract:

Polyaniline (PANI) is a candidate for electrocatalysis, and can be combined with metal nanoparticles to fabricate high-performance electrodes for electrochemical energy conversion and storage. However, its intrinsic properties appear to be dependent on the synthesis conditions so that from the majority of the reports, it is quite difficult to establish an overall performance trend. In this contribution, we report an extensive and systematic physicochemical and electrochemical screening of the potentiality of chemically synthesized PANI as an electrode material to provide an overall understanding of the effect of the entire synthesis conditions. We have integrated different methods (TGA-DSC, XRD, SEM, EDX, FTIR, BET, CHNS, XPS, CV, and EIS) to deeply examine the as-synthesized materials and interrogate their electrocatalytic efficiency towards hydrogen evolution reaction, which was chosen as a model reaction of critical importance for H_2 production from water splitting. It was found that all the synthesis parameters affect strongly the physical and electrochemical characteristics of the PANI-based materials. Specifically, XPS analysis contributed to identify the oxidation levels of the PANI samples on the basis of oxidizing agents. The outcomes provided by the study delineate a rational pathway for the further design and fabrication of PANI-based metal nanoparticles as advanced electrode materials.

Introduction

Hydrogen (H$_2$) is becoming a cornerstone not only for various industrial processes as a feedstock, but also as an energy carrier involved in the energy conversion and storage scenarios through the electrolysis and fuel cells.[1-3] One of the most effective and alternative route for its production with high purity is the water electrolysis.[3,4] Noble metals, and in particular the Pt-Ru-Ir series, have been considered as ideal electrocatalysts for the water electrolysis by reducing the overpotential during the electrocatalytic hydrogen evolution reaction (HER) and oxygen evolution reaction (OER), but the high cost and low earth abundance of these materials have limited their use in large-scale H$_2$ production technologies.[3,5-8] In such context, it is necessary to synthesize cost-effective materials suitable for HER as an alternative to Pt group metals (PGMs) based electrocatalysts. Among the electrode materials playing a significant role in the performance of energy storage and conversion devices, conducting polymers combined with metallic species are good candidates to elaborate high-performance electrocatalysts due to their interesting structural and physical properties, taking advantage of each component.[9-16] Among those conducting polymers, polyaniline (PANI)[17-19] is one of the most investigated material because of its high specific capacitance due to multi-redox reactions, its good electronic properties due to protonation and its high availability. In electrochemistry, PANI can directly act as "electrode" or indirectly as a supporting material. To date, PANI has proven to be an ideal supporting matrix for the immobilization of metal nanoparticles, resulting in electrode materials with superior performance and dispersive ability to prevent agglomeration of metal catalysts.[11,12,20-28]

Traditionally, PANI is synthesized by chemical or electrochemical methods, resulting in a powder or a thin film with interesting electron transfer abilities during electrochemical oxidation and reduction reactions in (bio)electrocatalysis.[19,25,26,29-41] As sketched in Figure 1, the polymer exists in three main oxidation states, well-identified by methods of cyclic voltammetry, a fully reduced state as leucoemeraldine base (LB), a semi-oxidized state as emeraldine base (EB) or emeraldine salt (ES) with an acid doping agent, and a fully oxidized state as pernigraniline base (PB).[42-44] The typical synthetic pathway for obtaining PANI involves the presence of an acid doping agent and an oxidizing agent that enables the polymerization of aniline (ANI, C$_6$H$_5$NH$_2$, consists of a phenyl group attached to an amino group). The oxidizing agents, such as APS, K$_2$Cr$_2$O$_7$, H$_2$O$_2$, KMnO$_4$, KI,[17,45-47] allow the elimination of a proton from the aniline monomer and the initiation of the polymerization through redox processes involving repetition of monomeric units.[48] The amount of the

oxidizing agent during the polymerization of PANI influences the amount of radical cations and thus the polymerization yield; however, an excess can lead to excessive oxidation of PANI, while a deficit may be insufficient to obtain the polymer.[49] Thus, the control of the [oxidizing agent]/[ANI] ratio is of critical importance. The insulating form of PANI, namely emeraldine base, consists in two amine nitrogen atoms followed by two imine nitrogen atoms and is a blue color (Figure 1b). The acidic doping agent (normal acid or Lewis acid), such as $HClO_4$, $FeCl_3$, NH_4BF_4, HCl, HNO_3, H_2SO_4, H_3PO_4,[20,44] allows the protonation of the imine nitrogen atoms of the emeraldine base to form the emeraldine salt (Figure 1c). It results in the generation of charge-carriers (a doubly charged bipolaron that spontaneously dissociates to give two polarons or radical cations) along the polymer backbone.[44,50] The hopping of the charge carriers through the polaron structure gives rise to a conducting polymer.[10-12] In addition to the influence of the amount and nature of the doping agent, the regular distribution of the counter-ions of the acid doping agent along the polymer backbone ensures a high structural regularity of the polymer backbone, and contributes to the increase of the charge carrier mobility. So, the doping process allows PANI to pass from insulator state to a conductive state with a crystalline (ordered) region responsible of its conductivity, dispersed in an amorphous (disordered) region.[29]

The chemical synthesis parameters based on the oxidizing agent, acid doping agent and counter anions have a great influence on the oxidation state and the doping level of PANI, resulting in various final morphologies and properties. Extensive literature is available regarding the influence of these reaction parameters on the synthesis of PANI, however, the results are difficult to compare because of different conditions of preparation, and the works dealing with the effect of all the reaction parameters related to the electrochemical characteristics of PANI are rarely available. This work was motivated by the desire to determine the optimal reaction conditions during the chemical oxidative synthesis of PANI in order to develop a noble metal-free PANI matrix with consistent quality and high electrical conduction, and to obtain an effective support of electrocatalysts. Given the high importance of PGMs-free electrocatalysts development for H_2 production, we used HER as the model reaction in acidic media. For that purpose, this work presents a systematic investigation aiming to establish the influence of the synthesis variables such as the doping agent, the oxidant agent, and oxidant/monomer ratio on the morphological, electrical and electrochemical properties of the resulted PANI-based materials. The entire results reveal that all the aforementioned reaction parameters affect strongly at different levels the structural

4

properties of the PANI materials, which in turn affect its efficiency towards HER in acidic media.

Experimental section

Chemicals and materials.

Aniline (ANI, 100%, Prolabo), hydrochloric acid (HCl, 37%, Carlo Erba), sulfuric acid (H_2SO_4, 98%, Sigma Aldrich), nitric acid (HNO_3, Cheminova, 60%) and phosphoric acid (H_3PO_4, 50%, Panreac) were used as doping agents. Ammonium persulfate (($NH_4)_2S_2O_8$, 98%, Biochem), potassium permanganate ($KMnO_4$, 99%, Fisher) and potassium dichromate ($K_2Cr_2O_7$, 99%, Prolabo) were used as oxidizing agents for the chemical aniline polymerization. Isopropanol (99.5%, Sigma Aldrich) and Nafion® suspension (5 wt%, sigma Aldrich) were used for the catalyst ink preparation. All chemicals were used without further purification, and electrolytic solutions used for polyaniline synthesis or for electrochemical characterizations were prepared freshly. All named ultrapure water (MQ) is provided by Milli-Q Millipore source (18.2 MΩ cm at 20 °C).

Preparation of PANI-based materials

The synthesis conditions are listed in Table S1. Typically, PANI was synthesized by the chemical oxidative polymerization as follows: a defined amount of aniline (ANI) is dissolved in 100 mL of an acid doping agent (HCl, H_2SO_4, H_3PO_4 or HNO_3) by stirring at room temperature. A solution consisting of 0.2 M of oxidizing agent (($NH_4)_2S_2O_8$, $KMnO_4$, or $K_2Cr_2O_7$) dissolved in another 100 mL of the above acid was added dropwise to the solution of aniline with vigorous stirring for 2 h at 5 °C. After 3 min, the color of the solution changed from colorless to dark green, indicating the beginning of the polymerization. The resulting PANI powder was filtered and washed with ultrapure water until the filtrate was colorless, and dried in an oven at 40 °C for one day.

Methods for physicochemical characterizations of the materials

X-ray diffraction (XRD) patterns were recorded by a DR-X-PRO-MPD-Philips diffractometer with $Cu_{K\alpha}$ radiation at the wavelength of 1.5406 Å, the voltage and tube current being 40 kV and 40 mA, respectively. Spectra were collected in a 2θ range from 5 to 80° at a room temperature. FTIR spectra were recorded on a Nicolet iS50 FTIR Spectrometer in the range of

4000-400 cm^{-1}, with a resolution of 4 cm^{-1}. The measurements were carried out at room temperature on the basis of 1 mg of PANI and 200 mg of KBr compacted into thin pellets using hydraulic press (5 tons). Thermogravimetric analysis (TGA) and differential scanning calorimetry (DSC) were performed with a SDT Q600 TA instruments on crucible of aluminum containing ca. 6 mg of material, in the temperature range of 25 to 500 °C with a heating rate of 10 °C min^{-1} and under air atmosphere (100 mL min^{-1}).The electrical conductivity was measured by four-point method at room temperature on pellets of the PANI (1 mm thickness and 13 mm diameter) using an Keithley Electrometers 2400 (Model LUCAS LABS, Pro 4-8400). The morphology of PANI powder was analyzed by scanning electron microscopy (SEM) on Hitachi S-4800 FEG, and the elemental analysis was obtained by energy dispersive X-ray spectroscopy (EDX) on the microscope ZEISS EVOHD 15, followed by 2D mapping of carbon (C) and nitrogen (N). The surface properties (porosity and the specific surface area (S_{BET})) were investegated by Brunauer-Emmett-Teller (BET) and distribution BJH measurements. N_2 adsorption-desorption isotherms were recorded at liquid N_2 temperature (77.3 K) using a Micromeritics ASAP 2020 instrument. CHNS analysis was performed on an Elementar vario MICRO cube. X-ray photoelectron spectroscopy (XPS) analyses (the analyzed surface and depth are of 300×700 µm^2 and 10 nm, respectively) were performed on a Kratos Axis Ultra DLD spectrometer equipped with a monochromatic radiation source Al Mono (Al$_{k\alpha}$ =1486.6 eV) operating at 150 W (15 kV and 10 mA). Data were recorded at a step of 1 eV (transition energy of 160 eV) and 0.1 eV (transition energy of 20 eV) for the survey and high-resolution spectra, respectively. The measured binding energy (BE) was corrected on the basis of the energy of C1s at 284.6 eV by using the CASA XPS software for the peaks fitting.The quantification was carried out from the peak area after correction with a suitable sensitivity factor.

Catalytic ink preparation.

The catalytic ink was prepared by mixing 2 mg of PANI powder, 180 µL of isopropanol and 20 µL of Nafion$^®$ suspension in a water ultrasonic bath for 20 min to form a homogenous ink. Then, 4 µL of the ink was coated on the surface of well-polished glassy carbon rotating disk electrode (GC-RDE, 5 mm diameter, 0.2 mg cm^{-2} loading) and dried under N_2 atmosphere at room temperature for 5 min. The GC-RDE was first polished with alumina at 3 µm, 1 µm and 0.05 µm, washed with ultrapure water, and a sonication in pure water for 5 min in order to remove all traces of alumina.

Electrochemical characterization by cyclic voltammetry

The electrochemical characterization was conducted in a conventional three-electrode cell using the SP150 potentiostat (Biologic Science Instruments). Ag/AgCl/KCl (3 M) was used as reference electrode and was separated from the solution by a Haber-Luggin capillary tip. The potentials were calibrated to the reversible hydrogen electrode (RHE) according to the calibration relationship E(V vs RHE) = E(Ag/AgCl) + (0.208 + 0.059×pH). A slab of glassy carbon of about 12 cm^2 was used as a counter electrode. The working electrode consists of a GC-RDE modified with the PANI based catalyst, which was characterized in 0.5 M H_2SO_4 (pH = 0.3) solution using cyclic voltammetry (CV) between 0.06 and 1.26 V vs RHE at 100 mV s^{-1}. The electrolyte solution was purged with N_2 over 20 min before measurements. All voltammograms are iR-free, i.e., corrected by the "potential drop" between the working and reference electrodes according to the relationship $E_{real} = E_{applied} - R_\Omega \times I$. R_Ω was obtained by the electrochemical impedance spectroscopy (EIS).

Electrochemical performance.

The electrocatalytic behavior of PANI-based electrodes towards HER was evaluated by linear sweep voltammetry (LSV). Before electrocatalytic measurements, each electrode was firstly cycled by CV for 30 cycles between 0.06 and 1.26 V vs RHE in N_2-saturated 0.5 M H_2SO_4, then LSV was conducted from the open circuit potential (OCP) to -1.024 V vs RHE at a scan rate of 5 mV s^{-1} and 900 rpm for 7 cycles. The Tafel slope value was calculated from the plot of the potential as a function of the current density in a logarithm-scale. The kinetic activity of the as-prepared electrodes towards HER was also estimated by EIS by scanning the frequencies from 200 kHz to 100 mHz (10 mV amplitude), at E_{appl} = -0.6 V vs RHE.

Accelerated ageing experiments.

Durability tests for the as-modified electrodes were carried out by LSV between OCP and -1.024 V vs RHE at a scan rate of 5 mV s^{-1} and 900 rpm for 500 cycles.

Results and Discussion

Influence of the doping agent on the physical, morphological and electrochemical properties

Effect of the doping agent concentration

The proton-based acid doping of the emeraldine base segment results in the protonation of the imine nitrogen atom in the backbone chain and gives emeraldine salt form with positive (proton) and negative (anion) charges. Thus, we firstly hypothesized that the doping agent concentration should affect the electrical conductivity of the conducting polymer. We especially aimed to study the polymerization process when using HCl as the proton-based acid doping agent, as a starting point for the preparation of PANI. To this end, Cl⁻ was chosen as the simplest and smallest counter-ion, in comparison to nitrate, sulfate and phosphate ones. Hence, the effects were likely to be easily accessed. To study the effect of the acid doping agent concentration on the polymer's properties, different PANI materials have been synthesized by the chemical oxidative polymerization in different concentration of HCl from 0.30 to 1.00 M, referred to as PANI-HCl0.30, PANI-HCl0.5, PANI-HCl0.75, and PANI-HCl1.00. We have chosen APS as the oxidizing agent with the molar ratio R = [APS]/[ANI] = 2 for [ANI] = 0.1 M as the best compromise. To evaluate the influence of those HCl conditions on the crystallinity and subsequently the conductivity and catalytic properties, we firstly characterize the homemade PANI-based materials by XRD. Figure 2a shows that the as-synthesized PANI-HCl materials exhibit 4 peaks at 2θ values of 8.88, 15.27, 20.80 and 25.54°, corresponding to (001), (011), (100) and (110) crystal planes, respectively, thus confirming the successful synthesis of a crystalline form of PANI, in agreement with the litterature.[51,52] Accordingly, the first peak at 8.88° is assigned to the d-spacing between the N atoms of adjacent main chain and the doping agent, the peaks at 15.27° and 20.80° are attributed to the parallel periodicity to the chains, whereas the peak at 25.50°, more intense, is ascribed to higher presence of PANI chains with perpendicular periodicity.[53-55] PANI in the un-doped state (polyaniline emeraldine base) is amorphous in nature,[56] and its crystallinity increases with increasing concentrations of the doping agent due to the incorporation of counter-ion (herein Cl⁻) and hydrostatic forces with protons.[57] This behavior is evidenced by the presence of a wider peak around 20.80° for the sample PANI-HCl0.30, thus reflecting a more amorphous structure. Moreover, the peak at 8.88°, mainly observed for the PANI-HCl0.50 and PANI-HCl0.75 samples, comes from a shorter distance between the counter-anion and the polymer chains, reflecting a higher order of PANI chains.[58] Besides, the values of β (full width at half-maximum), L_V (crystalline size) and d-spacing, estimated using Scherer and Bragg formula Eqs. 1 and 2, respectively[55,59] (Table S2), confirm the better mobility of charge carriers along the polymer main chain in the sample PANI-HCl0.50, meaning that it should have a higher electrical conductivity.[60]

$$d_{(hkl)} = \frac{\lambda}{2\sin\theta} \qquad [1]$$

$$L_V = \frac{k\lambda}{\beta\cos\theta} \qquad [2]$$

Where $\lambda (= 1.54060$ Å) is the X-ray wavelength, θ is the Bragg's angle, β(in radian) is the full width at half-maximum (FWHM) of the peak, k is a constant (≈ 0.9), L_V is the average crystallite size, d(hkl) is the inter-planar spacing of the crystallographic plane (hkl).

We next used FTIR spectroscopy to perform a deep characterization of the polymer materials. Figure 2b shows that increasing the HCl concentration results in spectra with a lower bands height in the region 2000-500 cm^{-1}, and broader bands in the region 3000-3800 cm^{-1}. The main peaks position of are resumed in Table S3. The characteristic peaks are observed around 3444 cm^{-1} (stretching vibration of N-H bond of the secondary amine[61]), 2925 and 2854 cm^{-1} (symmetric and asymmetric elongation of aliphatic C-H bonds), 1579 and 1497 cm^{-1} (stretching deformation of quinoid and benzenoid rings, respectively[58,62]), 1292 cm^{-1} (C-N stretching vibration), 1238 cm^{-1} (stretching vibration of delocalized polaronic structure C-N$^+$), 1142 cm^{-1} (vibration mode of protonated amines –NH$^+$= created during the doping process[63]), and 826 cm^{-1} (out-of-plane deformation of the bonds C-H of aromatic cycles). The shift of the bands corresponding to the quinoid and benzenoid rings to a lower wavenumber for the sample PANI-HCl0.50 confirms the higher degree of protonation of the material.[50] The profiles of TGA and DSC of PANI-HCl are reported in Figure 2c; the main characteristics are reported in Table S4. The upper temperature of 500 °C was fixed to avoid the combustion of carbon. The TGA curves reveal a common feature with a three-step mass loss for all samples. The first weight loss at about 120 °C is associated with the evaporation of water molecules that are adsorbed and trapped between the hydroscopic polymer chains and requiring a much higher temperature to remove them.[64,65] The peaks position is 142; 143, 143 and 147 °C for PANI-HCl0.30, PANI-HCl0.50, PANI-HCl0.75 and PANI-HCl1.0, respectively. For PANI-HCl1.0, the phenomenon occurs at much higher temperatures presumably because of the agglomerated morphology nature of the particles constituting the materials, whereby the removal of those solvent molecules embedded in the PANI's network is much hard. This will be fixed by the SEM observations. The second weight loss between 200 °C and 350 °C is ascribed to the elimination of the residual doping agent and the decomposition of smaller polyaniline fragments,[66] and the third loss above 330 °C is attributed to the degradation of the
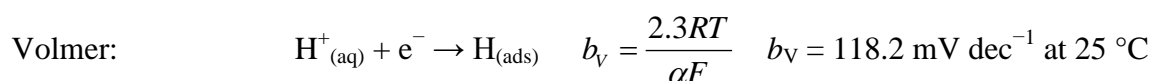
9

main PANI chains.[67] From DSC curves in Figure 2c, it can be observed that the evolution of PANI-HCl samples is similar and display four peaks corresponding to the endothermic process that needs energy in each decomposition stage (values reported in Table S4). The endothermic peaks between 130-150 °C and 160-200 °C correspond to the structural rearrangement and moisture desorption. The third endothermic peak between 230 °C and 320 °C can be associated to a mix phenomenon of "de-doping process", exclusion of residual anions (Cl⁻) from the polyaniline structure and the polymer reticulation, while the change at 422 °C is attributed to the structural degradation of the main PANI backbone.[68] The polymer reticulation is basically an exothermic process; however, as in the present case many phenomena occur simultaneously, the reticulation would be hidden. Indeed, the prevalence of the entire endothermic parts may imply that the reticulation of the polymer does not occur.

The forth physical method used herein to investigate those PAN-based carbon materials was the N_2 adsorption-desorption. This technique allows the assessment of the textural properties of porous materials by using N_2 as a probing molecule. Figure 2d depicts the N_2 adsorption-desorption isotherms (which belongs to the type IV) of representative PANI-HCl samples obtained at [HCl] = 0.50, 0.75 and 1.00 M. The hysterisis loop at a higher relative pressure that is characteristic of capillary condensation indicates the presence of mesopores. Quantitative data are reported in Table 1 and Table S4. The evaluated BET surface was 23, 25 and 6 m^2 g^{-1} for PANI-HCl0.50, PANI-HCl-0.75 and PANI-HCl1.00, respectively. From the pore size distribution measured by the BJH method (Figures S1), the polymers exhibit a mesopourous structure.[69,70] The pore volume is 0.13, 0.16 and 0.06 cm^3 g^{-1} for PANI-HCl0.50, PANI-HCl-0.75 and PANI-HCl1.00, respectively. The lowest specific surface area and pore volume values for PANI-HCl1.00 reinforces the presumption from the previous TGA results, which were suggesting a possible presence of agglomerated particles that reduce the available exposed surface. The strong impact of HCl concentration on the electrical conductivity (σ) of the PANI-HCl samples can be observed in Figure 2d (inset), and gathered in Table 1. σ increases from 3.7×10^{-4} to 0.25 S cm^{-1} for PANI-HCl0.30 to PANI-HCl0.50. This can be explained by the higher concentration of remaining protons capable of binding to N atoms of the imine units, thus promoting the formation of polarons/bipolarons between the polymer chains that are the charge carriers responsible for electrical conductivity of PANI.[71,72] For the concentration above 0.5 M HCl, the slight decrease in σ can be explained by a possible agglomerated morphology of the particles induced by the above excess protons binding to nitrogen atoms. From these physical characterizations of the HCl-depend properties of PANI, it can be concluded that the doping process allows the polymer to
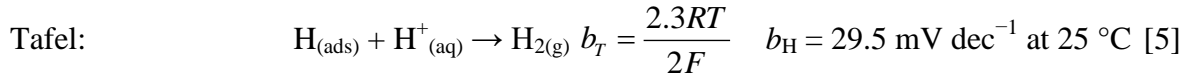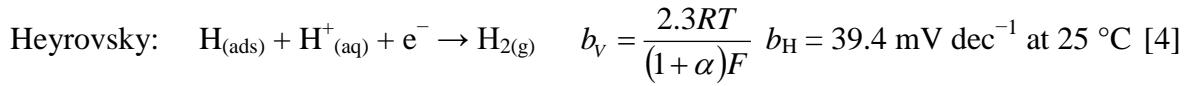
go from an insulating state to a semiconductor or conductive state. Conclusively, the best compromise for the starting points of [ANI] = 0.1 M and [APS]/[ANI] = 2 should be the use of HCl as the proton-based acid doping agent at the concentration of 0.5 M. This means that the molar ratio of HCl to ANI in the reactor should be 10:1.

The above studies show only the optimal conditions when these PANI-based materials are intended to be used as "raw material". To determine whether the conclusion could hold or not for the application in electrochemistry in aqueous solutions, we further electrochemically characterized them in H_2SO_4. Figure 2e shows the iR-free CV curves (2nd and 30th cycles) over the potential window of -0.06 to 1.26 V vs RHE. Compared to the blank glassy carbon electrode, the CV profiles of the PANI-based materials exhibit two characteristic redox processes, which correspond to the well-described oxidation states of PANI.[67,70,73] The PANI-HCl1.00 exhibits the lowest current density response, which could be substantiated by the above BET measurements. The pair of redox peaks located at 0.56/0.37 V vs RHE is ascribed to the electrochemical transition from the fully reduced form of PANI (leucoemeraldine) to the partially oxidized state (emeraldine salt), whereas the second pair of redox peak at 0.94/0.77 V vs RHE is attributed to the transition between the emeraldine salt and the fully oxidized form of PANI (pernigraniline).[73] After 30 cycles, the CV profiles present a steady-state response with only one redox system with oxidation/reduction peaks located at around 0.67 and 0.52 V vs RHE, respectively. It is argued that this behavior corresponds to an irreversible morphological transformation in the polymer associated with the reorganization of the polymer chains and mobility of the anions among the cycles.[44,74]

The electrocatalytic activity of the PANI-based materials for HER was evaluated by LSV and compared with pure GC-RDE support. It should be pointed out that the HER's mechanism on metal surfaces in acidic medium has been extensively studied,[75,76] and consists in three steps described by Eqs. 3-5. The Tafel slope value gives important information on the rate determining step (rds) in an electrochemical reaction. Indeed, the dominant reaction step in the HER process can be theoretically indicated by a Tafel slope. The latter can be obtained from experimental data of LSV or EIS and is broadly interpreted as the relation between the current density and the overpotential (dependence of steady-state current densities on a variety of overpotentials).

Volmer: $\quad\quad\quad\quad H^+_{(aq)} + e^- \rightarrow H_{(ads)} \quad b_V = \dfrac{2.3RT}{\alpha F} \quad b_V = 118.2 \text{ mV dec}^{-1} \text{ at } 25 \text{ °C}$

[3]

Heyrovsky: $\quad H_{(ads)} + H^+_{(aq)} + e^- \rightarrow H_{2(g)} \quad b_V = \dfrac{2.3RT}{(1+\alpha)F} \quad b_H = 39.4\ \text{mV dec}^{-1}$ at 25 °C [4]

Tafel: $\quad\quad\quad\quad\quad\quad H_{(ads)} + H^+_{(aq)} \rightarrow H_{2(g)}\ b_T = \dfrac{2.3RT}{2F} \quad b_H = 29.5\ \text{mV dec}^{-1}$ at 25 °C [5]

Where b_V, b_H and b_T are the Tafel slopes (mV dec^{-1}), α is the symmetry coefficient (typically, $\alpha = 0.5$), F is the Faraday constant (96 485 C mol^{-1}), R is the ideal gas constant (8.314 J K^{-1} mol^{-1}), and T is the absolute temperature (273.15 + °C).

Figure 2f shows that pristine GCE exhibits a very limited catalytic activity, while the PANI-HCl0.30 exhibits a catalytic activity closed to the PANI-HCl0.50, despite its low electrical conductivity, probably due to the protonation of the nitrogen atoms of amines units of polyaniline that occurs in the strong acid H_2SO_4. The overpotential required for driving a cathodic current density of 10 mA cm^{-2} for PANI-HCl0.30, PANI-HCl0.50, PANI-HCl0.75 and PANI-HCl1.0 is 0.74, 0.77, 0.77 and 0.85 V, respectively. This confirms the low performance of the sample PANI-HCl1.00. These catalytic activities are also assessed by the charge transfer resistance (R_{ct}) values obtained from Nyquist plots in Figure 2g and the Tafel slopes in Figure 2h. The modelling of EIS data by a representative equivalent electrical circuit (EEC) embedded in Figure 2g, i.e., $R_\Omega + Q_{CPE}//R_{ct}$ enables the determination of R_{ct} and Q_{CPE} (constant phase element).[77,78] The lack of homogeneity and mass transport is modelled with a Q_{CPE} while the metric of R_{ct} (inversely proportional to rate constant $k°$, thus to the exchange current density $j°$) is the ability of the electron-transfer electrode reaction to drive a large current density with a less driving force (overpotential).[79] For a given electrode, the lower R_{ct} is, the higher is the kinetic rate. The results gathered in Table 1 show that R_{ct} = 10, 20, 26 and 31 Ω cm^2 for [HCl] = 0.30, 0.50, 0.75 and 1.00, respectively. So, even though the sample PAN-HCl0.30 has a reduced "raw electrical conductivity" about two order of magnitude lower, the use of 0.5 M H_2SO_4 as the electrolyte enables to compensate the ionic conductivity. Furthermore, the determined mechanism descriptor of Tafel slope[80] is b = 120-150 mV dec^{-1}. This suggests that the *rds* of is the Volmer reaction (for a symmetry coefficient of α = 0.49-0.39) characterized by the limitation by the protons adsorption. On the basis of both metrics of the charge transfer resistance and the Tafel slope, the PANI-HCl1.0 has the lowest performance that may be supported by the previous TGA-DSC and BET results.

The above studies suggest that there may be a drastic morphological difference between the PANI materials obtained with [HCl] ≤ 0.50 M and [HCl] ≥ 1.00 M. Hence to gain further insights into the morphology, SEM analysis was undertaken for representative samples synthesized with [HCl] = 0.30, 0.50 and 1.00. Figure 3 shows that the PANI powders present an irregular granular morphology. The increase in HCl concentration to 1.00 M during the chemical polymerization results in an increase in the particle size, leading to agglomeration that result in lower BET surface and electrocatalytic performance. Since ANI was fixed to 0.1 M, the above concentrations correspond to a molar ratio [HCl]/[ANI] = 3, 5 and 10. It can be concluded that the presence of HCl is necessary to trigger the chemical polymerization process. But, too high concentration of protons relative to ANI (about 10) results in their excessive binding to N of the imine units. This promotes the formation of polarons/bipolarons between the polymer chains, which obviously leads to the formation of larger particles and reduced porosity. Based on all these physico-chemical and electrochemical screenings, the experimental conditions [HCl] = 0.5 M has been chosen as the best compromise for further investigations.

Effect of the ratio Oxidant/ANI

Having demonstrated the ability to use HCl to grow self-supported PANI particles, we sought to study the impact of APS more carefully. Indeed, given the important role of the oxidizing agent on the polymerization yield of PANI, its impact has been studied to modulate the catalytic efficiency. To these ends, the synthesis conditions consist in HCl as the doping agent at 0.5 M, APS as the oxidizing agent at [APS] = 0.2 M. Different PANI-based materials were synthesized using variable quantities of ANI through the ratio R = [APS]/[ANI] = 0.4-2.0 and referred to as PANI-R0.40, PANI-R0.5, PANI-R0.67, PANI-R1.00 and PANI-R2.00. The same set of methods was used to characterize the materials, XRD (Figure 4a), FTIR (Figure 4b), TGA-DSC (Figure 4c), N_2 adsorption-desorption isotherms and electrical conductivity (Figure 4d and Table 1). The profiles are similar to those of Figures 2a-d. The electrical conductivity (inset in Figure 4d) measurements show that the materials obtained for a molar ratio [APS]/[ANI] < 0.5, for instance the PANI-HCl-R0.4, have low conductivity. This is probably because of the low polymerization yield due to the deficiency of APS for oxidizing all the aniline monomer, which mainly results in the formation of shorter conjugation length of the polymer. The optimal conductivity of 1.39 S cm^{-1} is reached for the optimal ratio [APS]/[ANI] = 0.5. However, unlike the previous study where a plateau had been reached for larger [HCl]/[ANI] molar ratio, too much excess of APS induces an obvious deterioration of

13

the electrical conductivity (0.25 S cm^{-1} for [APS]/[ANI] = 2) due to the degradation by over-oxidation that produces shorter conjugated PANI chains.[49,81] These results can be confirmed by XRD data (Figure 4a and Table S2) that reveal the higher crystallinity degree of the polymer PANI-HCl-R0.5. FTIR spectra (Figure 4b) do not show any significant structure change with the variation of the ratio Oxidant/ANI. Contrary to what has been observed by several authors,[17,44] in our case, the evaluation of "the oxidation degree augmentation" of PANI for increase amount of APS could not be highlighted from the area ratio of the characteristic quinoid and benzenoid peaks. The N$_2$ adsorption-desorption isotherms and BET analysis (Figure 4d, Table S4) indicate that S_{BET} = 21, 26 and 23 m^2 g^{-1} for PANI-R0.50, PANI-R1.00 and PANI-R2.00, respectively. The pore volume is ca. 0.13 cm^3 g^{-1} for the three samples, meaning the same trends. At this stage of the study concerning the effect of the [APS]/[ANI] molar ratio, the best experimental conditions should be [HCl] = 0.5 M, [APS] = 0.2 M, and [APS]/[ANI] = 0.5 through [ANI] = 0.4 M.

Next, CV and LSV studies were carried out to probe the electrochemical and electrocatalytic properties of the samples. It should be mentioned that the optimized sample from the previous section is PANI-R2.00. Figure 4a shows that the highest current density for the redox peaks is reached for the sample PANI-R0.50. This behavior is substantiated by the performance towards HER (Figures 4f-g). PANI-HCl-R0.5 displays the best activity in terms of the overpotential at 10 mA cm^{-2}, decreasing from 0.77 to 0.69 V. The determined charge transfer resistance is R_{ct} = 15, 53, 42 and 20 Ω cm^2 for PANI-R0.50, PANI-R0.67, PANI-R1.00 and PANI-R2.00, respectively. This results highlight the fast electron transfer ability of the sample obtained with a [APS]/[ANI] molar ratio of 0.5. As previously, the evaluated Tafel slope (Figure 4h) of b = 110-131 mV dec^{-1} indicates that the *rds* is the Volmer reaction of the protons adsorption at the electrocatalytic surface. The SEM observations in Figure 5 for the materials obtained by [APS]/[ANI] = 0.5, 1 and 2 indicate that the aforementioned parameter affects marginally the morphology of the resulting polymers. This is consistent with the N 2 adsorption-desorption isotherms, in which the surface and pore volume are substantially the same. From the above investigations, we came with the conclusion that the optimal conditions should be [HCl] = 0.5 M, [APS] = 0.2 M, and [APS]/[ANI] = 0.5, i.e., [ANI] = 0.4 M and they have been chosen as the best compromise for the next step.

Effect of the nature of the doping agent

The electrical conductivity of conducting polymers depends also on the charge carriers' mobility, which depends on the size of the counter-ion of the doping agent attached to

polymer chain and the type of the formed polarons. Typically, a proton-based acid doping agent dissociates in water to generate protons and anions that could be inserted into the polymer matrix during the polymerization reaction and the positive charge is neutralized.[82] The acid dissociation constant and the counter-ion size may results in a difference in the protonation degree. During the synthesis, the anions having the smallest size easily diffused in the polymer matrix, thereby resulting in a higher doping level and high efficiency of the mobility process, which increase the conductivity.[83,84] In this context, the influence of the nature of the proton-based acid doping agent on the physicochemical and electrochemical properties of polyaniline was carefully studied during the synthesis of the polyaniline in the presence of the strong acids, H_2SO_4, H_3PO_4, HNO_3 and HCl, commonly used for in the synthesis and doping of PANI. Based on the previous conclusions, we have synthesized PANI-based materials using APS as the oxidizing agent at [APS] = 0.2 M, R = [APS]/[ANI] = 0.5 (i.e. ANI at 0.4 M) and different doping agents at a concentration of 0.5 M. The obtained materials are referred to as PANI-HCl, PANI-HNO$_3$, PANI-H$_2$SO$_4$ and PANI-H$_3$PO$_4$. The physicochemical characterizations are reported in Figures 6a-d, while the results from the electrochemistry are displayed in Figures 6e-h. Among the different acids, PANI-HCl exhibits by far the highest electrical conductivity (Figure 6d, inset). This property was confirmed by the data deduced from XRD (Figure 6a) that reveal the higher crystallinity degree and lower d-spacing for PANI-HCl (Table S2). The FTIR spectra analysis (Figure 6b and Table S3) supports the higher degree of protonation for PAN-HCl with a significant shift of the bands corresponding to the quinoid and benzenoid rings to lower wavenumbers.[50] No observable changes were observed for the N-H vibration modes with respect to hydrogen bonding. The thermal behavior of polyaniline shows a significant desorbed amount of the moisture for PANI-HCl about 17% and an improved thermal stability for PANI-HNO$_3$ with a total weight loss of 33%. For PANI-H$_2$SO$_4$ and PANI-H$_3$PO$_4$, a steeper weight loss is observed, suggesting a lower thermal stability of these polymers. Data collected from BET measurements by N$_2$ adsorption and desorption, and BJH methods (Figure 6d, Table S4, Figure S1) confirmed the mesoporous structure for all materials, and showed that PANI-HCl has the highest specific surface area of 21 m^2 g^{-1}, while PANI-H$_2$SO$_4$ has the lowest value of 16 m^2 g^{-1}.

Figure 6e shows the voltammograms of those PANI-based materials, which are similar for the entire samples and depicts the two characteristic pairs of redox peaks, corresponding to the oxidation and reduction process when scanning towards the anodic and the cathodic potential, respectively. It can be well observed that PANI-HCl and PANI-H$_3$PO$_4$ display

higher current densities compared to PANI-H$_2$SO$_4$ and PANI-HNO$_3$. From the HER's LSV polarization curves (Figure 6f) and Nyquist impedance plots at E_{appl} = -0.6 V vs RHE (Figure 6g), PANI-HCl exhibits the best activity towards HER with the lowest R_{ct} of 15 Ω cm^2, whereas PANI-H$_2$SO$_4$ shows the lowest performance with R_{ct} of 41 Ω cm^2. This time we can deduce that there is little variation in the slope of Tafel (Figure 6h), b = 122-130 mV dec^{-1} that denotes that the rate limiting step is still the Volmer reaction of protons. The SEM images (Figure 7) show a granular morphology contacted with some nanofibers domains for PANI-HCl, and more compacted and plate shape morphologies for the samples PANI-H$_2$SO$_4$, PANI-H$_3$PO$_4$ and PANI-HNO$_3$. Those SEM observations confirm the results of the N$_2$ adsorption-desorption isotherms, whereby no obvious difference was observed in terms of BET surface and total pore volume. So, it cannot be used as a "decision maker" to choose the best conditions to synthesize PANI-based materials. Combining the electrochemical and physico-chemical studies, HCl can be chosen as the best compromise to fabricate efficient PANI-based electrocatalyst.

Effect of the nature of the oxidant

As the last parameter of critical importance, the nature of the oxidizing agent on the PANI formation was studying with common types of oxidizing agents, namely APS ((NH$_4$)$_2$S$_2$O$_8$), KMnO$_4$ and K$_2$Cr$_2$O$_7$. We used the previously optimized condition of HCl as the proton-based doping agent at 0.5 M, ANI monomer at 0.4 M and the [oxidizing agent]/[ANI] molar ratio of 0.5, i.e., the oxidizing agent at 0.5 M. The as-fabricated materials are referred to as PANI-APS, PANI-K$_2$Cr$_2$O$_7$ and PANI-KMnO$_4$. The physical characterizations are reported in Figures 8a-d and electrochemical ones are displayed in Figures 8c-h. The crystallinity of the polymers has been examined by XRD and reported in Figure 8a. While PANI-APS is characterized by a partially crystalline structure with the typical peaks at 8.88°, 15.54°, 20.82° and 2θ = 25.50°, PANI-KMnO$_4$ and PANI-K$_2$Cr$_2$O$_7$ in contrast show broad Bragg diffraction peaks centered at 24.15° and 20.78°, respectively, which is characteristic of an amorphous structure. This result confirms the observed extremely low conductivity of PANI-KMnO$_4$ (2.1×10^{-3} S cm^{-1}) and PANI-K$_2$Cr$_2$O$_7$ (2.6×10^{-5} S cm^{-1}), compared to PANI-APS (Figure 8d, inset). This behavior may be explained by the low protonation level during the oxidation process in the presence of K$_2$Cr$_2$O$_7$ and KMnO$_4$. The particularity of APS is its high redox potential (2.01 V vs SHE) compared to the values of the redox potential of KMnO$_4$ and K$_2$Cr$_2$O$_7$ (1.51 and 1.33 V vs SHE, respectively), making it the best candidate for the chemical oxidative polymerization to yield PANI. From FTIR spectra in Figure 8b, the

increase of the oxidation degree of PANI with the different oxidant was not evaluated from the area ratio of the characteristic quinoid and benzenoid peaks, nevertheless, PANI-APS shows the higher degree of protonation with a significant shift of the main characteristic bands to lower wavenumbers.[50] From the thermal behavior of the three samples in Figure 8c, the weight loss process in the case of PANI-APS and PANI-KMnO$_4$ is characterized by three stages attributed to different structural changes in the polyaniline structure, as discussed above, while PANI-K$_2$Cr$_2$O$_7$ displays only two weight loss stages. The second step corresponding to the removal of doping agent has disappeared. The sample shows only 12% weight loss between 120-275 °C (Table S4), because of the low protonation degree, in addition, the faster weight loss and the absence of thermal stability zone were observed. The N$_2$ adsorption-desorption isotherms and BET analysis (Figure 8d, Table 1, Table S4) indicate that S_{BET} = 21, 11 and 2 m^2 g^{-1} for PANI-APS, PANI-K$_2$Cr$_2$O$_7$ and PANI-KMnO$_4$, respectively. The pore volume is 0.13, 0.04 and 0.01 cm^3 g^{-1} for the same trend, meaning a significantly increased "exposed surface area" for the PANI obtained under the synthesis condition with APS as the oxidizing agent. At this stage of the study concerning the type of oxidizing agent to be used in order to achieve the highest electrical conductivity and most importantly the surface area; APS should be used as the oxidizing agent at 0.2 M.

We next combined CV and LSV of HER to establish the voltammetry profiles and the electrocatalytic performance of the different samples derived from the use of the three types of oxidizing agents. From Figures 8e-h, the influence of the oxidant is clearly obvious. While PANI-APS presents the two typical redox transitions of leucoemeraldine/emeraldine-base and emeraldine-salt/pernigraniline with higher current densities, both PANI-K$_2$Cr$_2$O$_7$ and PANI-KMnO$_4$ display only one pairs of redox peaks at 0.78/0.41, 0.78/0.48 V vs RHE, with a potential difference (ΔE) of 0.37 and 0.30 V, respectively. Those large peak-to-peak differences can be interpreted as an increase of the irreversibility. The Figures 8e-f show that PANI-APS has the best activity towards HER (overpotential of 0.69 V at 10 mA cm^{-2}) with the lowest R_{ct} of 15 Ω cm^2, while PANI-K$_2$Cr$_2$O$_7$ presents a very weak catalytic activity with Tafel slope value of 178 mV dec^{-1}. The combination of the SEM observations (Figure 9) and the measured BET surfaces area (Table 1) demonstrate that the oxidant agent has a strong impact on the structural morphology of the PANI. PANI-APS has a granular morphology with an open structure (S_{BET} = 21 m^2 g^{-1}), while the PANI-K$_2$Cr$_2$O$_7$ exhibits a spherical morphology with irregular size distribution (S_{BET} = 11 m^2 g^{-1}), and PANI-KMnO$_4$ is characterized by a dense morphology with a very low porosity (S_{BET} = 2 m^2 g^{-1}). Based on these results, we have considered APS as the best oxidizing agent for the synthesis of efficient PANI-based

materials as "a potential catalyst" or "a supporting material of metallic nanoparticles" to be used in electrochemical applications. Conclusively, all those previous results show the ability to manipulate the synthesis conditions towards different polyaniline materials with different morphologies, electrical conductivity, electrochemical behaviors and electrocatalytic performance.

Compositional and surface screening

Having performed a thorough and step-by-step study of the synthesis conditions of PANI, we sought to study the materials composition more carefully. We specifically aimed to determine whether the theoretical chemical composition of the polyaniline is obtained or not and especially, the proportion of the different forms of PANI. For the atomic composition, we firstly utilized the EDX analysis. Figures 10a-h of representative materials qualitatively confirm the presence of C and N. The 2D maps confirm the successful synthesis of N-doped carbon materials with a uniform dispersion of carbon and nitrogen for each sample. As indicated in Figure 1, the theoretical atomic ratio C/N is 6. Quantitative EDX analysis in Figure 10i shows that an experimental proportion of 1 atom of N for 6 atoms of C is maintained in the entire PANI-based materials obtained from different conditions of [HCl] and [oxidizing agent]/[ANI]. Furthermore, EDX analysis of PANI-APS, PANI-$K_2Cr_2O_7$ and PANI-$KMnO_4$ samples showed the presence of S, Cr, and Mn species (not shown herein), which could also explain the observed morphology of the materials and their electrical and electrocatalytic properties. It is reported that sulfur improves the electrocatalytic activity of the HER.[85] On the contrary, Cr and Mn, whose oxide state within the current PANI is indisputable, exclude any catalytic effect. A further calcination step could enable obtaining a network of C, N and Cr/Mn that is more catalytically active, which is beyond the scope of the present study.

To deepen our knowledge about two of the key experimental parameters affecting drastically the electrocatalytic properties of PANI, we next carried out XPS analysis. Figure S2 shows the indexed survey XPS of the as-synthesized PANI-HCl0.5-R0.5-APS and PANI-HCl0.5-R1.0-APS to investigate the effect of [oxidizing agent]/[aniline] ratio, and of the PANI-HCl0.5-R0.5-$K_2Cr_2O_7$ to study the effect of the oxidizing agent. High-resolution C1s and N1s spectra are shown in Figure 11 and the extracted overall atomic composition is reported in Table S5. The presence of chlorine (0.5 at%) in both PANI materials synthesized with APS and its absence in the sample with $K_2Cr_2O_7$ will be explained below after the

examination of the N1s level. On the upside, the presence of S (1.6 at%) for APS-based materials and chromium (2.7 at%) for the $K_2Cr_2O_7$-based material was expected. The C/N atomic ratio of 6.4-7.0 obtained by XPS, which analyzes only a nanoscale domain (~10 nm) of the sample, confirms the previous EDX results and definitely supports the successful retention of the aniline-based blocks (6 atoms of C for 1 atom of N). Figures 11a-c display the different components of high-resolution XPS of C1s while quantitative atomic composition is reported in Table S6. The peak centered at ca. 284.6 eV belongs to the graphitic carbon (sp^2-hybridized carbon atoms, C=C)[86,87] while that at ~285.6 eV can be associated with the formation of C-N chemical bonds as well as C-O function.[87-89] The peaks situated at 286.5 and 288.1 eV can be assigned to the carbonyl (C=O) and carboxylate (O-C=O) functions, respectively. For graphene-based materials, it is well-known that the peak at 290-291 eV belongs to the $\pi \rightarrow \pi*$ shake-up satellite peak.[87,90] However, looking closely at the possible structures of the PANI-based materials (Figure 1), this $\pi \rightarrow \pi*$ shake-up satellite can be split up to two peaks depending on the oxidation state of the PANI, herein at 289.6 and 292.0 eV for PANI-HCl0.5-R0.5-APS or PANI-HCl0.5-R0.5-APS (in agreement with the litterature[89]). A single peak is observed for PANI-HCl0.5-R0.5-$K_2Cr_2O_7$. This is in line with the chlorine result and can indicate the change in the oxidation state of the PANI. Specifically, a deep analysis of N1s (Figures 11d-f) reveals four main components, known to be the imine ($-N=C$, N1) at ca. 398.3 eV, the amine ($-NH-C$, N2) at ~399.9 eV, the polaron ($-NH_\bullet^+-C$, N3) at 400.5-401.1 eV, and the bipolaron ($-NH^+=C$, N4) at 402.7-403.3 eV.[89,91-97] Additionally, the peak at 406.1-406.6 eV is assigned to the $\pi \rightarrow \pi*$ shake-up satellite (N5) of the doublet presents on some nitrogen.[98,99] The atomic distribution of those nitrogen atoms into N1-N5 species is reported in Figure 12a and Table S7. By calculating the atomic ratio (N1+N3+N4)/(N1+N2+N3+N4), it is possible to further determine the oxidation state of the PANI.[95-97,100] More precisely, a value of 0.5 indicates an intermediate oxidation stage of nitrogen in the PANI (emeraldine form), a value closed to 1 signifies a higher concentration of quinoid groups and therefore a highly oxidized form (pernigraniline), and a ratio below 0.5 denotes the predominance of a highly reduced PANI (leucoemeraldine). As it can be also observed in Figure 12a, the evaluated ratio is 0.48, 0.41 and 0.66 for PANI-HCl0.5-R0.5-APS, PANI-HCl0.5-R1.0-APS, and PANI-HCl0.5-R0.5-$K_2Cr_2O_7$, respectively. In other words, the PANI obtained by using APS as an oxidizing agent is in the form of emeraldine while a pernigraniline form results from the use of $K_2Cr_2O_7$. Interestingly, the polaron/bipolaron amount is 43, 38, and 23 at% for PANI-HCl0.5-R0.5-APS, PANI-HCl0.5-

R1.0-APS, and PANI-HCl0.5-R0.5-$K_2Cr_2O_7$, respectively. In other words, the high amount of the polaron species is accompanied by the presence of choline. It is well-known that these species are responsible of the electrical conductivity (σ) of the polyaniline.[10-12] Thus, it is not surprising that from Figures 4d and 8d, the values are σ = 1.39, 0.64 and 2.6×10^{-5} S cm^{-1} for PANI-HCl0.5-R0.5-APS, PANI-HCl0.5-R1.0-APS, and PANI-HCl0.5-R0.5-$K_2Cr_2O_7$, respectively. Conclusively, this XPS study validates the previous physical and electrochemical data and supports the critical importance of the synthesis inputs.

The utilization of both EDX and XPS techniques does not allow accessing the amount of hydrogen atoms. Even if this was the case, a real composition would not be possible because those methods do not perform the entire bulk analysis quantitatively. So, we alternatively utilized the "CHNS analysis" to determine the real bulk composition of C, N and H (Table S8). The results in terms of C/N and C/H atomic ratios are reported in Figure 12b. It also reveals that the C/N ratio is about 6, while the C/H ratio is ca. 0.9, indicating the presence of a large amount of N and H atoms. However, the inevitable presence of water molecules adsorbed and trapped between polyaniline chains results in an overestimation of the H atoms in the polyaniline materials since the theoretical ratio was expected to be between 1.20 and 1.50 depending on the oxidation state of the polyaniline (Figure 1 and Table S7).

Accelerated ageing effect on the electrochemical properties

After the previous set of characterization, we finally sought to gain deeper insights about the behavior of the PANI upon the potential cycling. The electrochemical accelerated ageing procedures by potential/current cycling or by fixing potential/current enable to anticipate the behavior of a material during real use. Given the electrochemical behavior of polyaniline as previously noted by voltammetry, we used LSV to interrogate the durability of two representative PANI samples. Experiments were performed with PANI-R0.50 and PANI-R1.00 by scanning the electrode potential between OCP and -1.024 V vs RHE at a scan rate of 5 mV s^{-1} and 900 rpm for 500 cycles and by recording the potential of OCP 30 s between two cycles to reach a relative stabilized electrode after the removal of the H_2 bubbles from the electrode surface. The obtained results are reported in Figures 13a-b. It should perhaps be reiterated that the previous LSV of HER are those obtained for the 7th LSV, in order to save time. The evolution of the overpotential required to reach the metric current density of 10 mA cm^{-2} (Figure 13a) is in agreement with the previous behavior of the CVs. suggesting stable HER activity in acid media. After 300 cycles, the overpotential is about 500 mV for the

electrode PAN-R0.5, i.e., 150 mV lower than the electrode PANI-R1. This is in agreement with the previous results. It should be noted that the blank experiment of a glassy carbon electrode does not show any significant change of the activity. So, the observed positive change could be assigned to a structural change at the polymer itself. Further deeper postmortem scrutinizing could provide insights about the trend. In the literature, one of the methods identified for boosting the electrocatalytic activity of polyaniline towards the HER in an aqueous medium is the introduction of species such as Co and Ni, making it possible to reach a current density of 10 mA cm^{-2} with overpotential of 100-300 mV.[20,24,25] For instance, Feng et al.[25] have demonstrated that the multi-composition PANI/CoP material increases the hydrogen evolution electrocatalysis in 0.5 M H_2SO_4, whereby the PANI can effectively capture H^+ from hydronium ions to form protonated amine groups, having a higher positive charge density than those of hydronium ions and can be electro-reduced easily. Even though the concept is beyond the scope of the present work, the introduction of metals followed by the materials calcination should results in electrocatalysts with high performance. In this case, the knowledge provided by the present study on the oxidation state of polyaniline would be crucial. Indeed, the transformation at high temperatures of the latter into a nanostructured carbon network containing or not nitrogen depends strongly on how those nitrogen atoms were bound to the carbon as well as the type of carbon-carbon bounds in the parent structure.

Conclusion

The present work was aimed to provide a complete understanding of the effect of the synthesis conditions on the physical and electrochemical properties of the polyaniline (PANI) obtained from the conventional chemical polymerization. Different physicochemical (TGA-DSC, FTIR, XRD, SEM, EDX, CHNS, BET, and XPS) and electrochemical (voltammetry and impedance spectrometry) methods have been integrated to characterize the as-synthesized polyaniline materials and to interrogate the property-to-performance relationship. The electrocatalytic hydrogen evolution reaction (HER) in acidic media has been chosen as a model reaction. Indeed, the electrochemical production of H_2, an essential feedstock for industrial processes and energy carrier for fuel cells, appears to be one of the sustainable power-to-X scenarios to significantly reduce the dependence on conventional energy sources based on fossil fuels. Our outcomes show that the morphology, the conductivity, and the electrochemical performance of the polyaniline are mainly determined by the synthesis conditions. Specifically, the proton-based acid doping agent and the oxidant affect the degree

of crystallinity, the inter-chain separation, the oxidation state, the degree of doping and further the density of charge carriers and their mobility along the polymer backbone, which in turn affects the electrical properties of PANI. The XPS results show that the use of APS as an oxidizing agent leads to the formation of the emeraldine (the best [oxidizing agent]/[aniline] ratio being 0.5), while a pernigraniline form arises from the use of $K_2Cr_2O_7$. After 500 cycles of the electrode potential cycling, the synthesized PANI using the ammonium persulfate (APS) as the oxidizing agent and HCl as the doping acid has a stable electrode potential of -0.5 V vs RHE at the current density of -10 mA cm^{-2} for a Tafel slope of ca. 120 mV dec^{-1}. The present study contributes to advances in the use of polyaniline, as an emerging conductive polymer for the design of cost-effective electrode materials for electrochemical energy conversion and storage applications. Specifically, it paves pathways for the development of efficient nanocatalysts for the electrocatalysis, whereby noble metal-free elements could be embedded in a matrix of an optimized conducting polymer to yield nitrogen and metals doped carbon nanostructured networks.

Acknowledgements

References

1. I. Staffell, D. Scamman, A. V. Abad, P. Balcombe, P. E. Dodds, P. Ekins, N. Shah and K. R. Ward, *Energy Environ. Sci.*, **12**, 463 (2019).
2. M. A. Rosen and S. Koohi-Fayegh, *Energy, Ecology and Environment*, **1**, 10 (2016).
3. V. R. Stamenkovic, D. Strmcnik, P. P. Lopes and N. M. Markovic, *Nat. Mater.*, **16**, 57 (2017).
4. S. S. Kumar and V. Himabindu, *Materials Science for Energy Technologies*, **2**, 442 (2019).
5. N. Cheng, S. Stambula, D. Wang, M. N. Banis, J. Liu, A. Riese, B. Xiao, R. Li, T.-K. Sham and L.-M. Liu, *Nat. Commun.*, **7**, Article number: 13638 (2016).
6. S. Anantharaj, S. R. Ede, K. Sakthikumar, K. Karthick, S. Mishra and S. Kundu, *ACS Catal.*, **6**, 8069 (2016).
7. N. Armaroli and V. Balzani, *ChemSusChem*, **4**, 21 (2011).
8. J. H. Montoya, L. C. Seitz, P. Chakthranont, A. Vojvodic, T. F. Jaramillo and J. K. Norskov, *Nat. Mater.*, **16**, 70 (2017).
9. R. Aydın and F. Köleli, *Prog. Org. Coat.*, **56**, 76 (2006).
10. Y. T. Dong, J. X. Feng and G. R. Li, *Macromol. Chem. Phys.*, **218**, 1700359 (2017).

11. H. Wang, J. Lin and Z. X. Shen, *Journal of Science: Advanced Materials and Devices*, **1**, 225 (2016).

12. K. E. Ramohlola, G. R. Monana, M. J. Hato, K. D. Modibane, K. M. Molapo, M. Masikini, S. B. Mduli and E. I. Iwuoha, *Composites, Part B*, **137**, 129 (2018).

13. S. Ghosh, T. Maiyalagan and R. N. Basu, *Nanoscale*, **8**, 6921 (2016).

14. S. Ghosh, S. Bera, S. Bysakh and R. N. Basu, *Sustainable Energy Fuels*, **1**, 1148 (2017).

15. S. Ghosh, S. Bera, S. Bysakh and R. N. Basu, *ACS Appl. Mater. Interfaces.*, **9**, 33775 (2017).

16. S. Ghosh, A.-L. Teillout, D. Floresyona, P. de Oliveira, A. Hagège and H. Remita, *Int. J. Hydrogen Energy*, **40**, 4951 (2015).

17. A. Pron, F. Genoud, C. Menardo and M. Nechtschein, *Synth. Met.*, **24**, 193 (1988).

18. H. S. Kolla, S. P. Surwade, X. Zhang, A. G. MacDiarmid and S. K. Manohar, *J. Am. Chem. Soc.*, **127**, 16770 (2005).

19. Z. A. Boeva and V. G. Sergeyev, *Polym. Sci., Ser. C*, **56**, 144 (2014).

20. D. A. Dalla Corte, C. Torres, P. dos Santos Correa, E. S. Rieder and C. de Fraga Malfatti, *Int. J. Hydrogen Energy*, **37**, 3025 (2012).

21. S. Ding, P. He, W. Feng, L. Li, G. Zhang, J. Chen, F. Dong and H. He, *J. Phys. Chem. Solids*, **91**, 41 (2016).

22. S. Padmapriya, S. Harinipriya, V. Sudha, D. Kumar, S. Pal and B. Chaubey, *Int. J. Hydrogen Energy*, **42**, 20453 (2017).

23. S. Padmapriya, S. Harinipriya, K. Jaidev, V. Sudha, D. Kumar and S. Pal, *Int. J. Energy Res.*, **42**, 1196 (2018).

24. C. Torres, B. Moreno, E. Chinarro and C. de Fraga Malfatti, *Int. J. Hydrogen Energy*, **42**, 20410 (2017).

25. J.-X. Feng, S.-Y. Tong, Y.-X. Tong and G.-R. Li, *J. Am. Chem. Soc.*, **140**, 5118 (2018).

26. W. Bai, X. Zhang and J. Zheng, *J. Electrochem. Soc.*, **166**, H336 (2019).

27. A. Leone, W. Marino and B. R. Scharifker, *J. Electrochem. Soc.*, **139**, 438 (1992).

28. S. Bao, M. Du, M. Zhang, H. Zhu, P. Wang, T. Yang and M. Zou, *J. Electrochem. Soc.*, **161**, H816 (2014).

29. S. Bhadra, D. Khastgir, N. K. Singha and J. H. Lee, *Prog. Polym. Sci.*, **34**, 783 (2009).

30. W. T. Napporn, J. M. Léger and C. Lamy, *J. Electroanal. Chem.*, **408**, 141 (1996).

31. A. Kelaidopoulou, A. Papoutsis, G. Kokkinidis, W. T. Napporn, J. M. Leger and C. Lamy, *J. Appl. Electrochem.*, **29**, 101 (1999).

32. E. C. Venancio, W. T. Napporn and A. J. Motheo, *Electrochim. Acta*, **47**, 1495 (2002).

33. G. Wu, K. L. More, C. M. Johnston and P. Zelenay, *Science*, **332**, 443 (2011).

34. S. Xu and S. D. Minteer, *ACS Catal.*, **4**, 2241 (2014).

35. J. H. Shendkar, V. V. Jadhav, P. V. Shinde, R. S. Mane and C. O'Dwyer, *Heliyon*, **4**, e00801 (2018).

36. R. Silva, D. Voiry, M. Chhowalla and T. Asefa, *J. Am. Chem. Soc.*, **135**, 7823 (2013).

37. M. S. Matseke, T. S. Munonde, K. Mallick and H. Zheng, *Electrocatalysis*, **10**, 436 (2019).

38. H. Lee, M. J. Kim, T. Lim, Y.-E. Sung, H.-J. Kim, H.-N. Lee, O. J. Kwon and Y.-H. Cho, *Sci. Rep.*, **7**, Article number: 5396 (2017).

39. C. Cao, L. Wei, G. Wang, J. Liu, Q. Zhai and J. Shen, *Inorg. Chem. Front.*, **4**, 1930 (2017).

40. Y. Liu, J. Li, F. Li, W. Li, H. Yang, X. Zhang, Y. Liu and J. Ma, *J. Mater. Chem. A*, **4**, 4472 (2016).

41. U. Martinez, E. F. Holby, S. K. Babu, K. Artyushkova, L. Lin, S. Choudhury, G. M. Purdy and P. Zelenay, *J. Electrochem. Soc.*, **166**, F3136 (2019).
42. S.-B. Yoon, E.-H. Yoon and K.-B. Kim, *J. Power Sources*, **196**, 10791 (2011).
43. J. De Albuquerque, L. Mattoso, R. Faria, J. Masters and A. MacDiarmid, *Synth. Met.*, **146**, 1 (2004).
44. M. Canales, J. Torras, G. Fabregat, A. Meneguzzi and C. Alemán, *J. Phys. Chem. B*, **118**, 11552 (2014).
45. J. Niziol, M. Sniechowski, A. Podraza-Guba and J. Pielichowski, *Polym. Bull.*, **66**, 761 (2011).
46. W. K. Maser, R. Sainz, M. T. Martínez and A. M. Benito, *Contrib. Sci.*, 187 (2008).
47. M. Neetika, J. Rajni, P. K. Singh, B. Bhattacharya, V. Singh and S. Tomar, *High Perform. Polym.*, **29**, 266 (2017).
48. N. Gospodinova and L. Terlemezyan, *Prog. Polym. Sci.*, **23**, 1443 (1998).
49. J. Deng, X. Wang, J. Guo and P. Liu, *Ind. Eng. Chem. Res.*, **53**, 13680 (2014).
50. P. Kong, P. Liu, Z. Ge, H. Tan, L. Pei, J. Wang, P. Zhu, X. Gu, Z. Zheng and Z. Li, *Catal. Sci. Technol.*, **9**, 753 (2019).
51. T. Chen, C. Dong, X. Li and J. Gao, *Polym. Degrad. Stab.*, **94**, 1788 (2009).
52. H. Zeghioud, S. Lamouri, Y. Mahmoud and T. Hadj-Ali, *J. Serb. Chem. Soc.*, **80**, 1435 (2015).
53. M. Khalid, M. A. Tumelero, I. Brandt, V. C. Zoldan, J. J. Acuña and A. A. Pasa, *Indian J. Mater. Sci.*, **2013** (2013).
54. B. Rajender and S. Palaniappan, *New J. Chem.*, **39**, 5382 (2015).
55. H. R. Tantawy, D. E. Aston, J. R. Smith and J. L. Young, *ACS Appl. Mater. Interfaces.*, **5**, 4648 (2013).
56. M. Canales and C. Alemán, *J. Phys. Chem. B*, **114**, 9771 (2010).
57. J. Pouget, M. Jozefowicz, A. e. a. Epstein, X. Tang and A. MacDiarmid, *Macromolecules*, **24**, 779 (1991).
58. F. Zeng, Z. Qin, B. Liang, T. Li, N. Liu and M. Zhu, *Prog. Nat. Sci.: Mater. Int.*, **25**, 512 (2015).
59. P. Chutia and A. Kumar, *Phys. B: Condens. Matter*, **436**, 200 (2014).
60. S. Sinha, S. Bhadra and D. Khastgir, *J. Appl. Polym. Sci.*, **112**, 3135 (2009).
61. U. Sidwaba, U. Feleni, H. Makelane, E. Nxusani, L. Wilson, S. Qakala, C. Rassie, M. Masikini, T. Waryo and R. F. Ajayi, in *Journal of Nano Research*, p. 281 (2016).
62. Y. K. Choi, H. J. Kim, S. R. Kim, Y. M. Cho and D. J. Ahn, *Macromolecules*, **50**, 3164 (2017).
63. K. L. Bhowmik, K. Deb, A. Bera, R. K. Nath and B. Saha, *J. Phys. Chem. C*, **120**, 5855 (2016).
64. B. Lubentsov and O. Timofeeva, *Synth. Met.*, **45**, 235 (1991).
65. E. C. Gomes and M. A. S. Oliveira, *Am. J. Polym. Sci.*, **2**, 5 (2012).
66. X. Wang, D. Liu, J. Deng, X. Duan, J. Guo and P. Liu, *RSC Adv.*, **5**, 78545 (2015).
67. A.-u.-H. A. Shah, M. Kamran, S. Bilal and R. Ullah, *Materials*, **12**, 1527 (2019).
68. A. Parveen and A. S. Roy, *Adv. Mater. Lett.*, **4**, 696 (2013).
69. S. Shahabuddin, N. Muhamad Sarih, S. Mohamad and J. Joon Ching, *Polymers*, **8**, 27 (2016).
70. M. M. Sk, C. Y. Yue and R. K. Jena, *RSC Adv.*, **4**, 5188 (2014).
71. J. Wu, Y. Sun, W. Xu and Q. Zhang, *Synth. Met.*, **189**, 177 (2014).
72. D. W. Hatchett, M. Josowicz and J. Janata, *J. Phys. Chem. B*, **103**, 10992 (1999).
73. J. Xing, M. Liao, C. Zhang, M. Yin, D. Li and Y. Song, *Phys. Chem. Chem. Phys.*, **19**, 14030 (2017).

74. J. Casanovas, M. Canales, C. A. Ferreira and C. Alemán, *J. Phys. Chem. A*, **113**, 8795 (2009).

75. A. Eftekhari, *Int. J. Hydrogen Energy*, **42**, 11053 (2017).

76. K. Ojha, S. Saha, P. Dagar and A. K. Ganguli, *Phys. Chem. Chem. Phys.*, **20**, 6777 (2018).

77. A. Lasia, *Electrochemical Impedance Spectroscopy and its Applications*, p. 367, Springer-Verlag, New York, NY, USA (2014).

78. M. E. Orazem and B. Tribollet, *Electrochemical Impedance Spectroscopy*, p. 367, John Wiley & Sons, Inc. , Hoboken, New Jersey, USA (2017).

79. A. J. Bard and L. R. Faulkner, *Electrochemical Methods: Fundamentals and Applications*, p. 850, John Wiley & Sons, Inc., USA (2001).

80. J. P. N. Ross, V. Radmilovic and N. M. Markovic, in *Catalysis and Electrocatalysis at Nanoparticle Surfaces*, A. Wieckowski, E. R. Savinova and C. G. Vayenas Editors, p. 311, CRC Press, New York, USA (2003).

81. W. Hammed, M. Rahman, H. Mahmud, R. Yahya and K. Sulaiman, *Des. Monomers Polym.*, **20**, 368 (2017).

82. A. Kawahara, S. Tsuji and H. Honda, *Int. Res. J. Pure Appl. Chem.*, 1 (2016).

83. J. Shen, S. Shahid, A. Sarihan, D. A. Patterson and E. A. Emanuelsson, *Sep. Purif. Technol.*, **204**, 336 (2018).

84. H. F. Alesary, H. K. Ismail, A. F. Khudhair and M. Q. Mohammed, *Orient. J. Chem.*, **34**, 2525 (2018).

85. X. Zou and Y. Zhang, *Chem. Soc. Rev.*, **44**, 5148 (2015).

86. A. M. Andersson, D. P. Abraham, R. Haasch, S. MacLaren, J. Liu and K. Amine, *J. Electrochem. Soc.*, **149**, A1358 (2002).

87. K. Kumar, C. Canaff, J. Rousseau, S. Arii-Clacens, T. W. Napporn, A. Habrioux and K. B. Kokoh, *J. Phys. Chem. C*, **120**, 7949 (2016).

88. S. Stankovich, D. A. Dikin, R. D. Piner, K. A. Kohlhaas, A. Kleinhammes, Y. Jia, Y. Wu, S. T. Nguyen and R. S. Ruoff, *Carbon*, **45**, 1558 (2007).

89. R. Rajagopalan and J. O. Iroh, *Appl. Surf. Sci.*, **218**, 58 (2003).

90. X. Fan, W. Peng, Y. Li, X. Li, S. Wang, G. Zhang and F. Zhang, *Adv. Mater.*, **20**, 4490 (2008).

91. H. S. O. Chan, P. K. H. Ho, S. C. Ng, B. T. G. Tan and K. L. Tan, *J. Am. Chem. Soc.*, **117**, 8517 (1995).

92. X.-R. Zeng and T.-M. Ko, *Polymer*, **39**, 1187 (1998).

93. B. Sreedhar, M. Sairam, D. K. Chattopadhyay, P. P. Mitra and D. V. M. Rao, *J. Appl. Polym. Sci.*, **101**, 499 (2006).

94. X. L. Wei, M. Fahlman and A. J. Epstein, *Macromolecules*, **32**, 3114 (1999).

95. Y. Y. Smolin, M. Soroush and K. K. S. Lau, *Beilstein Journal of Nanotechnology*, **8**, 1266 (2017).

96. J. Yue and A. J. Epstein, *Macromolecules*, **24**, 4441 (1991).

97. H. R. Tantawy, B.-A. F. Kengne, D. N. McIlroy, T. Nguyen, D. Heo, Y. Qiang and D. E. Aston, *J. Appl. Phys.*, **118**, 175501 (2015).

98. M. P. Keane, A. N. de Brito, N. Correia, S. Svensson and S. Lunell, *Chem. Phys*, **155**, 379 (1991).

99. G. Soto, E. C. Samano, R. Machorro, M. H. Farías and L. Cota-Araiza, *Appl. Surf. Sci.*, **183**, 246 (2001).

100. S.-A. Chen and G.-W. Hwang, *J. Am. Chem. Soc.*, **117**, 10055 (1995).

Table 1. BET surface area, electrical conductivity (EC), and EIS analysis of the as-prepared PANI-based materials.

Entry	BET	EC	EIS			
	$S_{BET}(m^2\,g^{-1})$	$\sigma(S\,cm^{-1})$	$R_{\Omega}(\Omega\,cm^2)$	$R_{ct}(\Omega\,cm^2)$	$Q_{CPE}(\mu F\,s^{a-1})$	a
PANI-HCl0.30_APS_R2	–	3.7×10^{-4}	1.4	10.3	1.6	0.90
PANI-HCl0.50_APS_R2	23	0.25	1.6	20.1	1.6	0.92
PANI-HCl0.75_APS_R2	25	0.18	1.3	26.2	1.2	0.92
PANI-HCl1.00_APS_R2	6	0.15	1.3	31.4	1.2	0.91
PANI-R0.50_HCl0.50_APS	21	1.39	2.4	15.2	1.8	0.90
PANI-R0.67_HCl0.50_APS	–	0.75	2.2	41.5	1.8	0.94
PANI-R1.00_HCl0.50_APS	26	0.64	2.1	17.5	1.8	0.94
PANI-R2.00_HCl0.50_APS	23	0.25	1.6	20.1	1.6	0.89
PANI-HCl_R0.50_APS	21	1.39	2.4	15.2	1.8	0.90
PANI-HNO$_3$_R0.50_APS	20	0.26	2.0	20.2	1.5	0.89
PANI-H$_2$SO$_4$_R0.50_APS	16	0.50	2.0	41.5	1.4	0.91
PANI-H$_3$PO$_4$_R0.50_APS	18	0.33	2.3	18.2	1.4	0.92
PANI-APS_R0.50_HCl	21	1.39	2.4	15.2	1.8	0.90
PANI-K$_2$Cr$_2$O$_7$_R0.50_HCl	11	2.6×10^{-5}	2.0	345.0	1.4	0.90
PANI-KMnO$_4$_R0.50_HCl	2	2.1×10^{-3}	1.4	75.4	1.3	0.93

Figure 1 (single column)
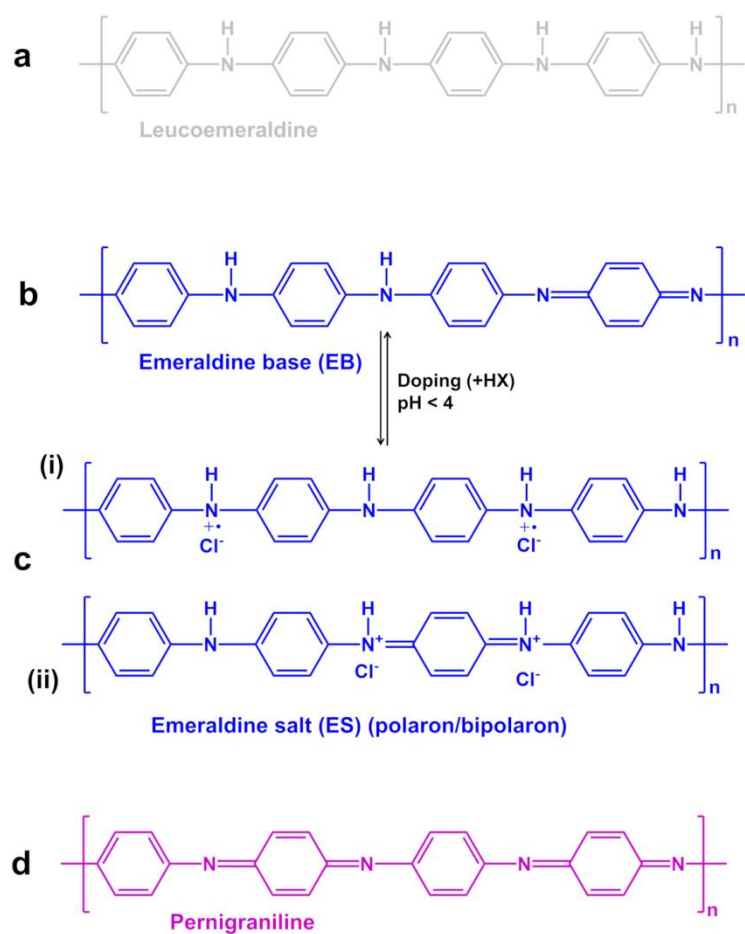
Figure 1. Chemical structure of the different types of polyaniline. (a) leucoemeraldine (LE, colorless or white in color, 100% C-NH-C amine bonds, i.e. fully reduced state), (b) emeraldine base (EB, blue in color, 50% C-NH-C amine bonds and 50% C=N-C imine bonds), emeraldine salt (ES, green in color) after doping giving rise to polaron and bipolaron structures, (c) pernigraniline (PG, purple in color, 100% C=N-C imine bonds, fully oxidized state). n = polymerization degree.
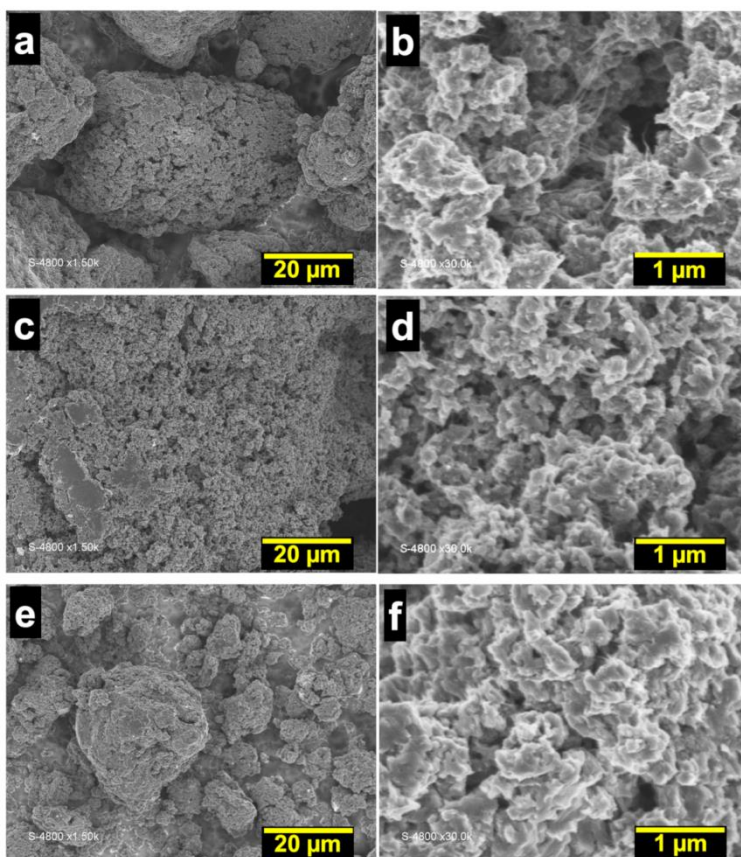
Figure 2 (double column)
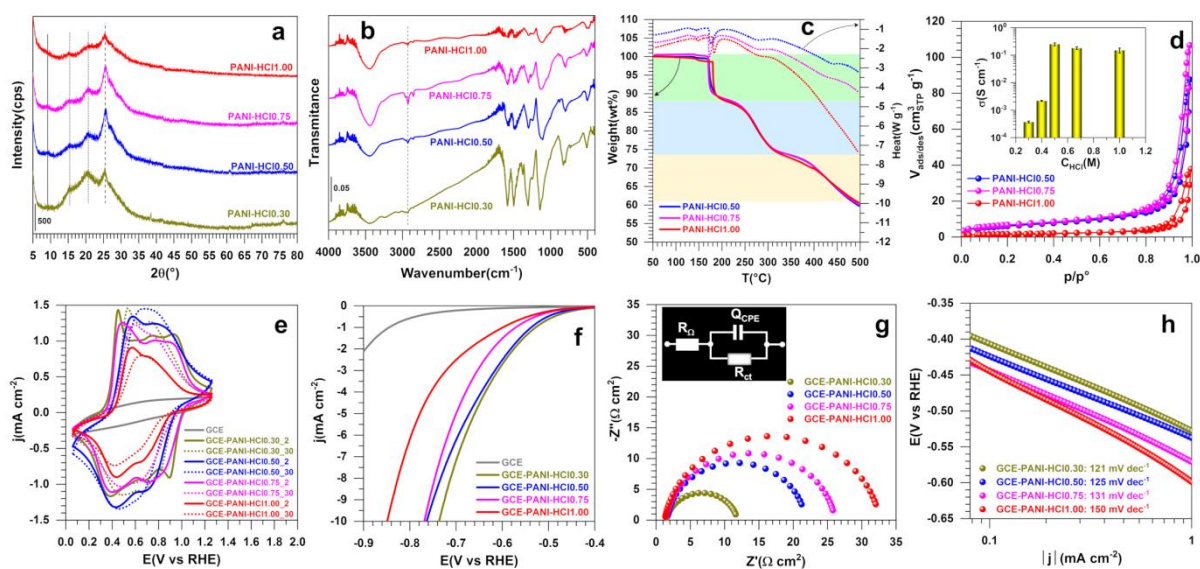
Figure 2. (a-d) Properties and (e-h) performance (in 0.5 M H$_2$SO$_4$ at 25 °C) of the as-synthesized PANI-based materials at different concentrations of [HCl] ranging from 0.3 to 1.00 M and using APS as the oxidizing agent at R = [APS]/[ANI] = 2 while [ANI] = 0.1 M. (a) XRD patterns, (b) FTIR spectra, (c) TGA-DSC curves, (d) N$_2$ adsorption-desorption isotherms: the inset shows electrical conductivity measurement data, (e) iR-free CVs recorded at 100 mV s^{-1}, (f) iR-free 7th LSVs recorded at 5 mV s^{-1}, (g) Complex-plane Nyquist impedance plots at E$_{appl}$ = -0.6 V vs RHE: the inset shows the use EEC for data fitting that is R$_\Omega$+Q$_{CPE}$//R$_{ct}$, (h) Tafel plots from the panel (f).

Figure 3 (single column)
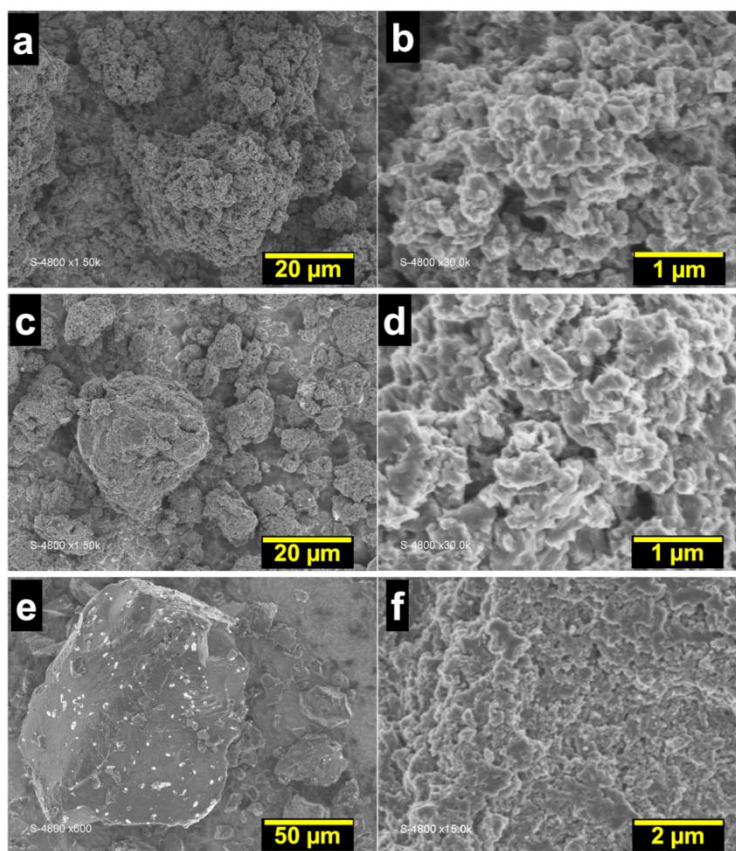
Figure 3. Overview (a, c, e) and near view (b, d, f) SEM micrographs of the as-synthesized PANI at different concentrations of [HCl]: (a, b) 0.3 M, (c, d) 0.50 M and (e, f) 1.00 M. Oxidizing agent = APS, R = [APS]/[ANI] = 2 and [ANI] = 0.1 M.
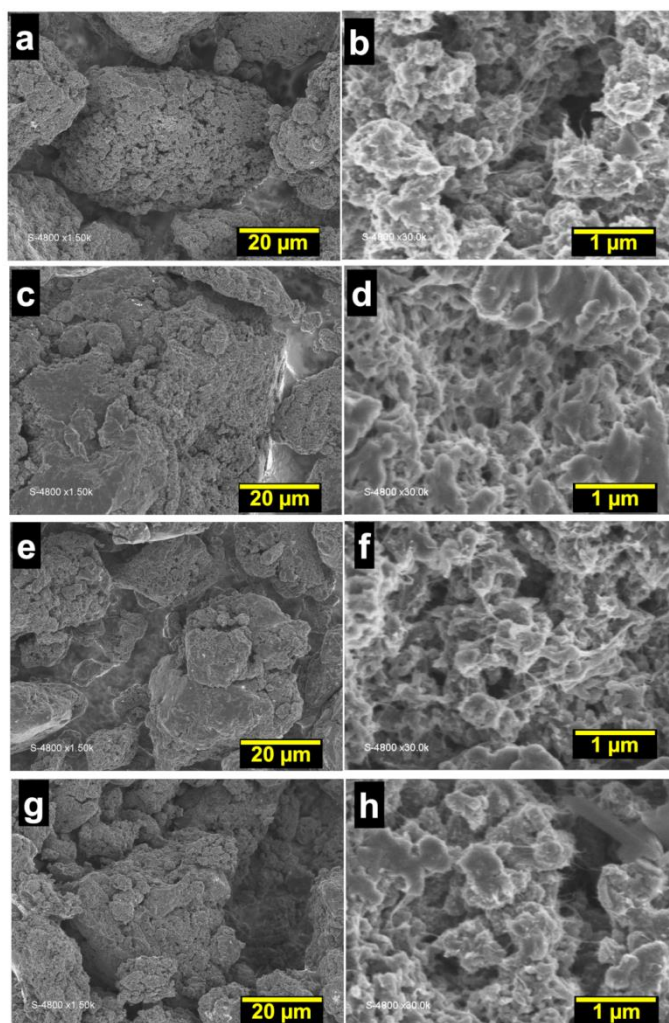
Figure 4 (double column)
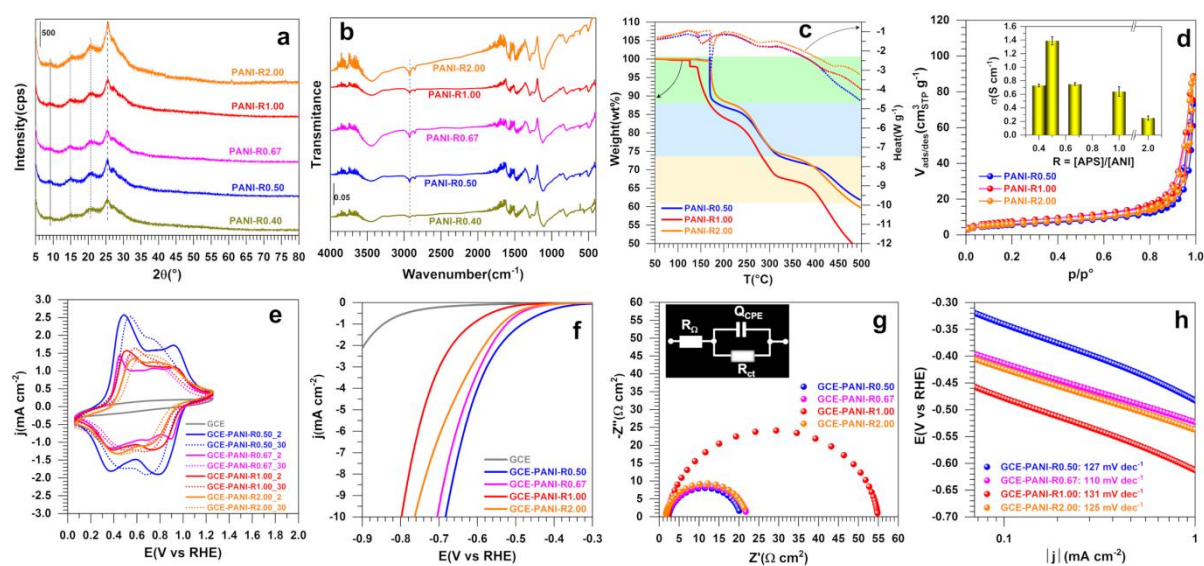
Figure 4. (a-d) Properties and (e-h) performance (in 0.5 M H$_2$SO$_4$ at 25 °C) of the as-synthesized PANI-based materials using HCl as the doping agent at 0.5 M and APS as the oxidizing agent at [APS] = 0.2 M for different amounts of ANI through the ratio R = [APS]/[ANI]. (a) XRD patterns, (b) FTIR spectra, (c) TGA-DSC curves, (d) N$_2$ adsorption-desorption isotherms: the inset shows electrical conductivity measurement data, (e) iR-free CVs recorded at 100 mV s^{-1}, (f) iR-free 7th LSVs recorded at 5 mV s^{-1}, (g) Complex-plane Nyquist impedance plots at E$_{appl}$ = -0.6 V vs RHE: the inset shows the use EEC for data fitting that is R$_\Omega$+Q$_{CPE}$//R$_{ct}$, (h) Tafel plots from the panel (f).

Figure 5 (single column)

Figure 5. Overview (a, c, e) and near view (b, d, f) SEM micrographs of the as-synthesized using HCl as the doping agent at 0.5 M and APS as the oxidizing agent at [APS] = 0.2 M for different amounts of ANI through the ratio R = [APS]/[ANI]. (a, b) R = 0.5, (c, d) R = 1 and (e, f) R = 2. Oxidizing agent = APS and doping agent = HCl at 0.5 M.
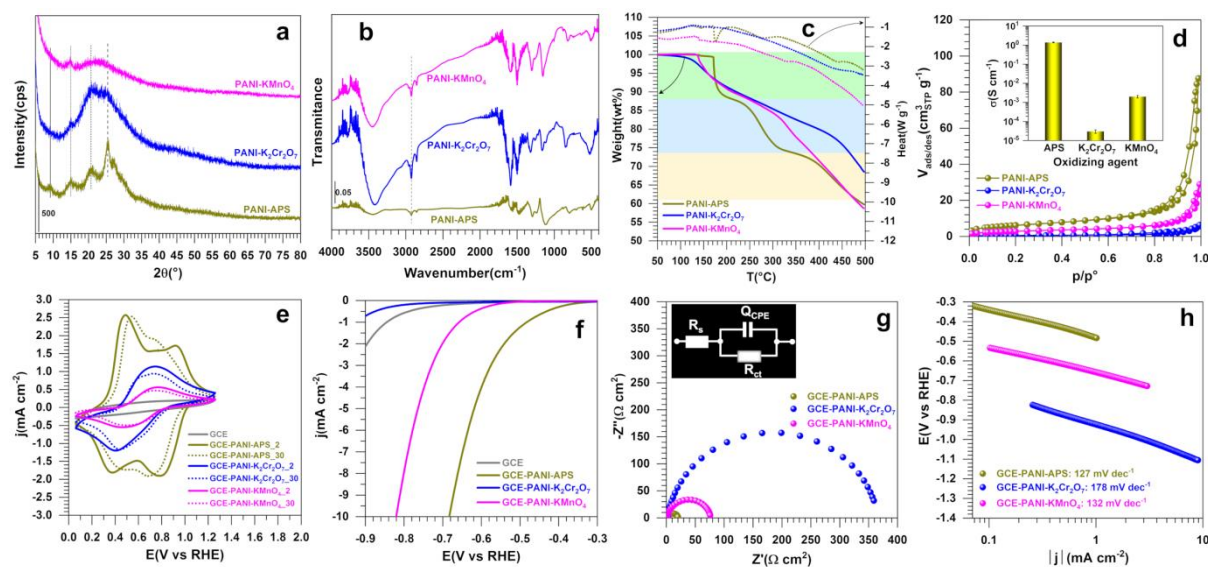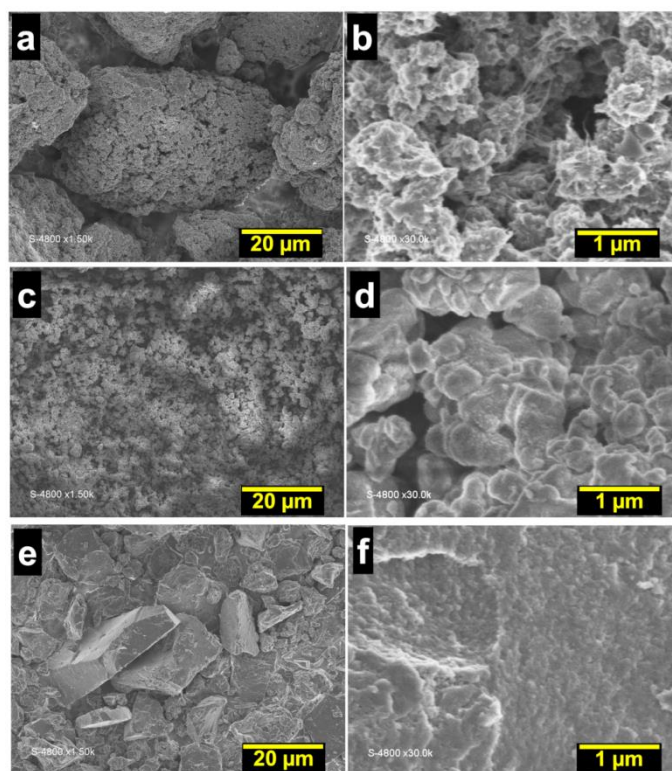
Figure 6 (double column)
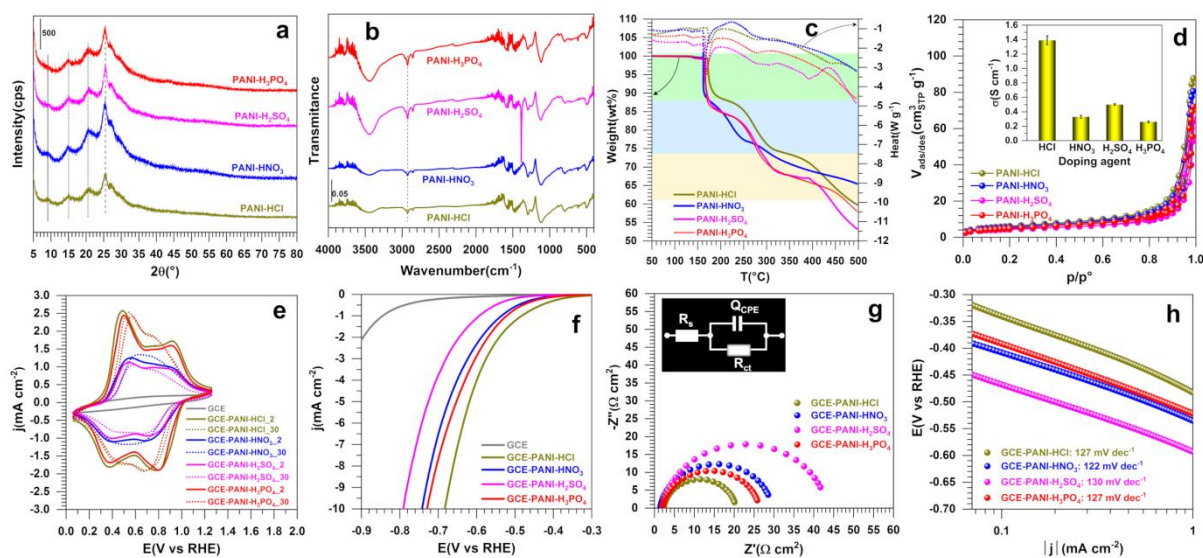
Figure 6. (a-d) Properties and (e-h) performance (in 0.5 M H_2SO_4 at 25 °C) of the as-synthesized PANI-based materials using different doping agents at a concentration of 0.5 M, APS as the oxidizing agent at [APS] = 0.2 M and R = [APS]/[ANI] = 0.5. (a) XRD patterns, (b) FTIR spectra, (c) TGA-DSC curves, (d) N_2 adsorption-desorption isotherms: the inset shows electrical conductivity measurement data, (e) iR-free CVs recorded at 100 mV s^{-1}, (f) iR-free 7th LSVs recorded at 5 mV s^{-1}, (g) Complex-plane Nyquist impedance plots at E_{appl} = -0.6 V vs RHE: the inset shows the use EEC for data fitting that is $R_\Omega+Q_{CPE}//R_{ct}$, (h) Tafel plots from the panel (f).

Figure 7 (single column)

Figure 7. Overview (a, c, e, g) and near view (b, d, f, h) SEM micrographs of the as-synthesized PANI with doping agents at 0.5 M: (a, b) HCl, (c, d) HNO_3, (e, f) H_2SO_4 and (g, h) H_3PO_4. Oxidizing agent = APS and R = [APS]/[ANI] = 0.5.

Figure 8 (double column)

Figure 8. (a-d) Properties and (e-h) performance (in 0.5 M H_2SO_4 at 25 °C) of the as-synthesized PANI-based materials using different oxidizing agents at R = [oxidizing agent]/[ANI] = 0.5, HCl as the doping agent at 0.5 M and [ANI] = 0.4 M. (a) XRD patterns, (b) FTIR spectra, (c) TGA-DSC curves, (d) N_2 adsorption-desorption isotherms: the inset shows electrical conductivity measurement data, (e) iR-free CVs recorded at 100 mV s^{-1}, (f) iR-free 7th LSVs recorded at 5 mV s^{-1}, (g) Complex-plane Nyquist impedance plots at E_{appl} = -0.6 V vs RHE: the inset shows the use EEC for data fitting that is $R_\Omega + Q_{CPE}//R_{ct}$, (h) Tafel plots from panels (f).

Figure 9 (single column)

Figure 9. Overview (a, c, e) and near view (b, d, f) SEM micrographs of the as-synthesized PANI with oxidizing agents at the ratio R = [oxidizing agent]/[ANI] = 0.5 and [ANI] = 0.4 M. (a, b) APS, (c, d) $K_2Cr_2O_7$, and (e, f) $KMnO_4$. Doping agent = HCl at 0.5 M.

Figure 10 (double column)
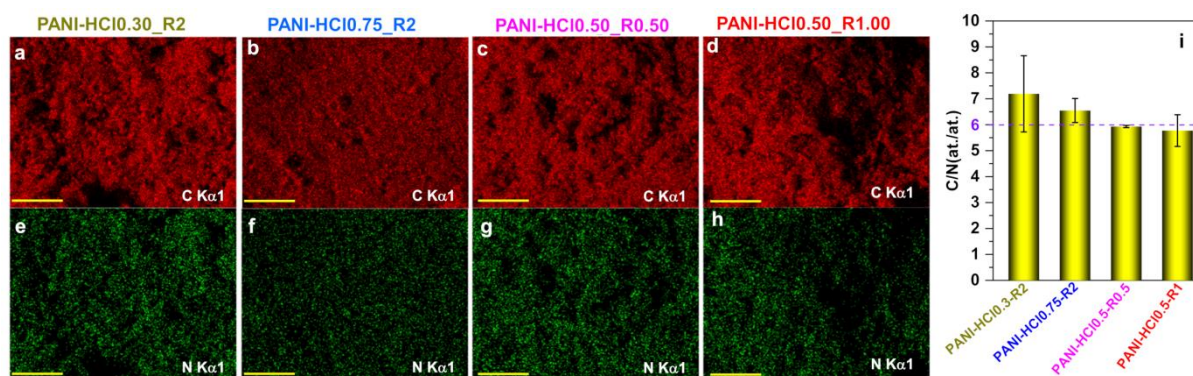
Figure 10. Compositional analysis by EDX of the as-synthesized PANI-based materials, (a-h) elemental mapping images (scale bare = 25 μm) and (i) quantitative results. (a, b, e, f) Effect of HCl concentration, (c, d, g, h) Effect of the ratio R = [APS]/[ANI], (i) atomic ratio C/N: the horizontal dashed line represents the theoretical value of 1 atom of N for 6 atoms of C.
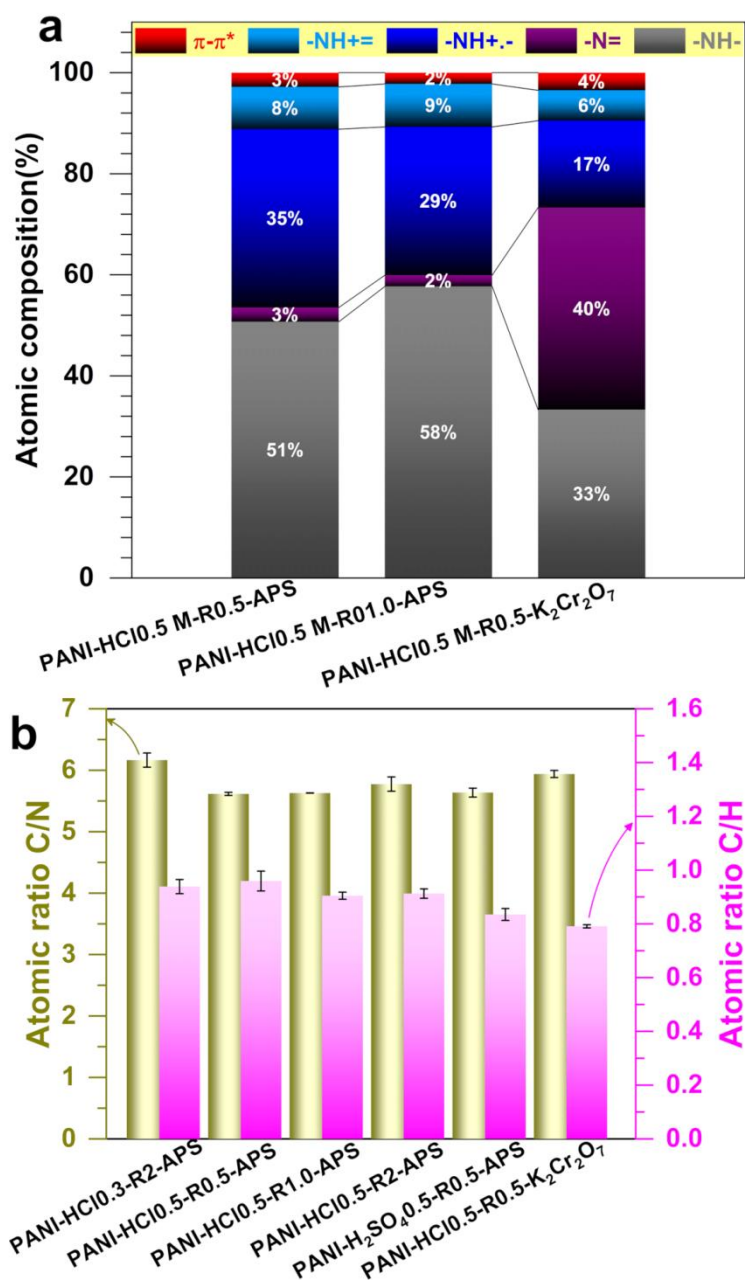
Figure 11 (double column)
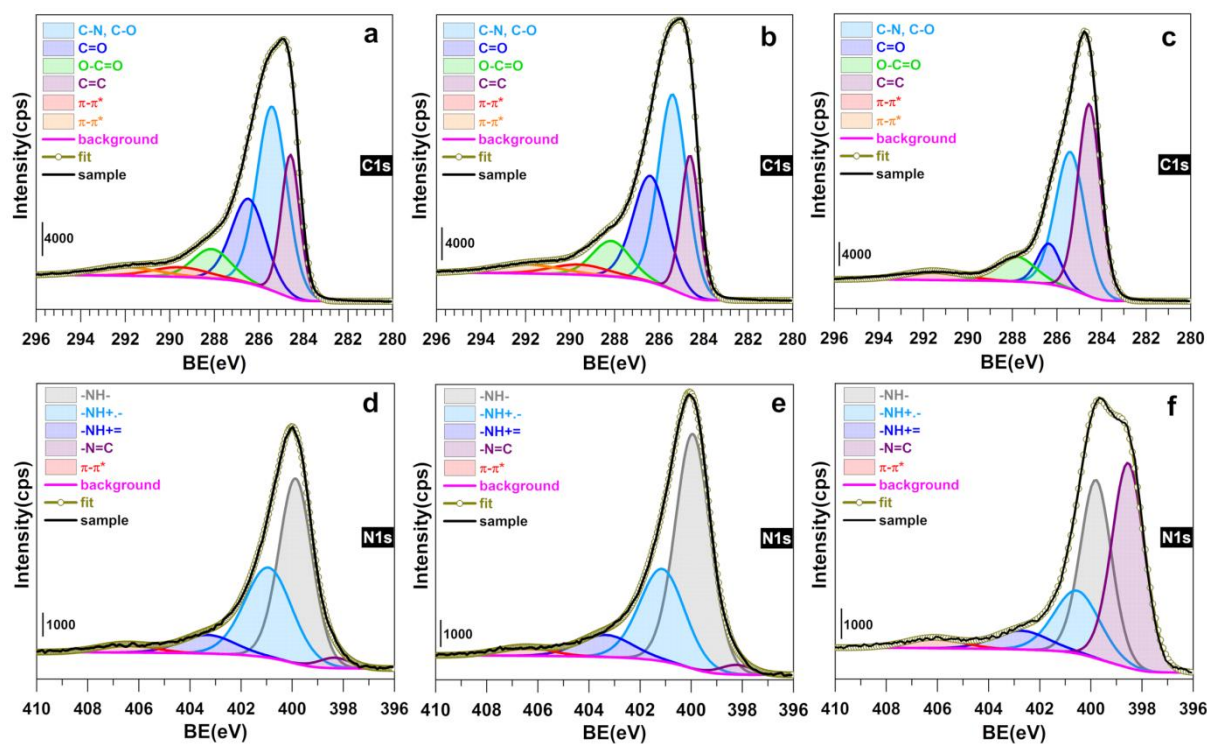
Figure 11. High-resolution XPS spectra of the core level C1s (a-c) and N1s (d-f) obtained for the as-synthesized materials: (a, d) PANI-HCl0.5-R0.5-APS, (b, e) PANI-HCl0.5-R1-APS, and (c, f) PANI-HCl0.5-R0.5-K$_2$Cr$_2$O$_7$.

Figure 12 (single column)

Figure 12. (a) Surface atomic composition of the different types of N species as-determined from XPS of N1s. (b) CHNS analysis of materials: atomic ratios of C/N (Left *y*-axis) and C/H (Right *y*-axis).
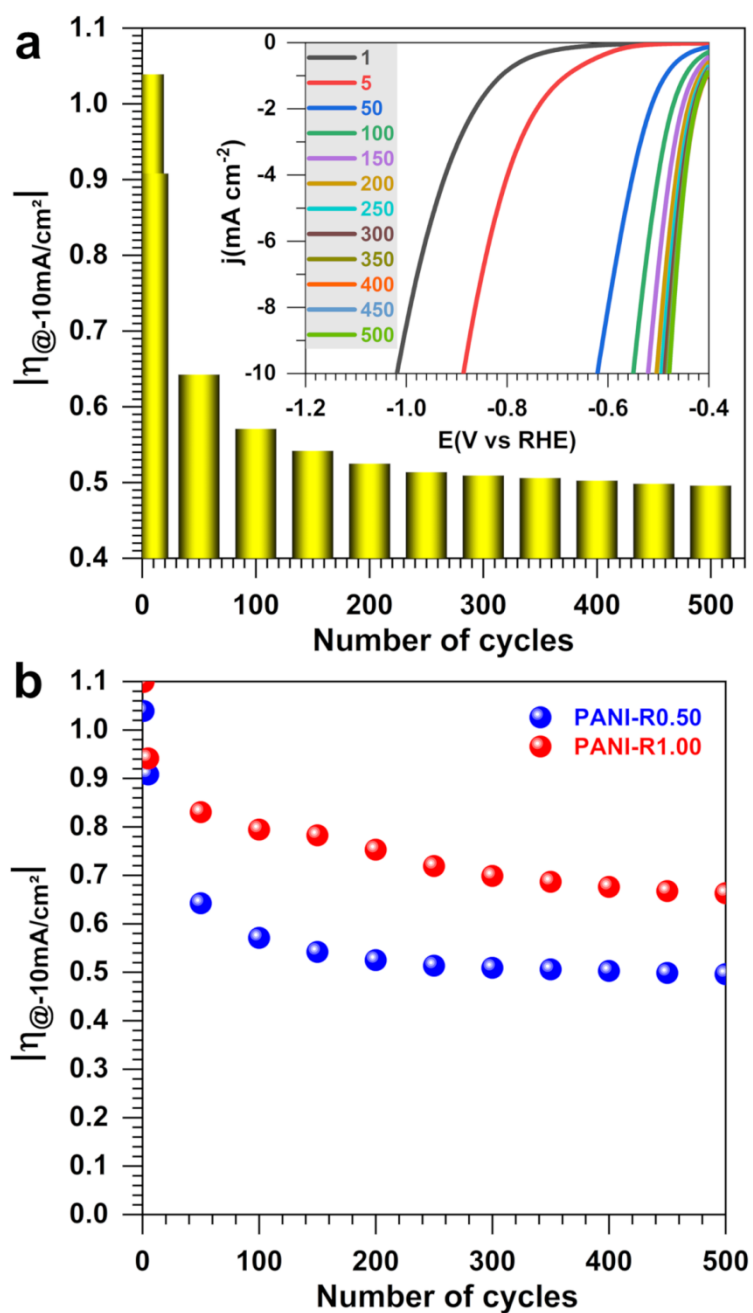
Figure 13. Accelerated potential cycling in 0.5 M H_2SO_4 at 25 °C for the as-synthesized PANI-based materials using HCl as the doping agent at 0.5 M and APS as the oxidizing agent at different amounts through the ratio R = [APS]/[ANI]. (a) LSV recorded at 5 mV s^{-1} and inset the overpotential at j = -10 mA cm^{-2} for R = 0.5. (b) Behaviors of the overpotential at j = -10 mA cm^{-2} from LSV recorded at 5 mV s^{-1}.